# Infinitesimal cranking for triaxial angular-momentum-projected configuration-mixing calculations and its application to the $\gamma$ vibrational band

Shingo Tagami and Yoshifumi R. Shimizu
*Department of Physics, Graduate School of Science, Kyushu University, Fukuoka 819-0395, Japan*
(Received 26 December 2015; published 29 February 2016)

Inclusion of time-odd components into the wave function is important for a reliable description of rotational motion by the angular-momentum-projection method; the cranking procedure with infinitesimal rotational frequency is an efficient way to realize it. In the present work we investigate the effect of this infinitesimal cranking for a triaxially deformed nucleus, where there are three independent cranking axes. It is found that the effects of cranking about three axes on the triaxial energy spectrum are quite different and inclusion of all of them considerably modifies the resultant spectrum from the one obtained without cranking. Employing the Gogny D1S force as an effective interaction, we apply the method to the calculation of the multiple $\gamma$ vibrational bands in $^{164}$Er as a typical example, where the angular-momentum-projected configuration mixing with respect to the triaxial shape degree of freedom is performed. With this method, both the $K = 0$ and the $K = 4$ two-phonon $\gamma$ vibrational bands are obtained with considerable anharmonicity. Reasonably good agreement, though not perfect, is obtained for both the spectrum and transition probabilities with rather small average triaxial deformation $\gamma \approx 9^\circ$ for the ground-state rotational band. The relation to the wobbling motion at high-spin states is also briefly discussed.

DOI: 10.1103/PhysRevC.93.024323

## I. INTRODUCTION

The angular-momentum-projection method is a fully microscopic means to recover the rotational invariance, which is broken in the self-consistently determined nuclear mean-field, e.g., by the Hartree-Fock-Bogoliubov (HFB) calculation. Although a nice rotational spectrum is obtained by the projection from one intrinsic mean-field, it often happens that the moment of inertia is smaller in comparison with the experimental data as long as the projection is performed from the time-reversal invariant mean-field state. Inclusion of the time-odd components is important for a realistic description of nuclear rotational motion, and one of the efficient ways to realize it is the so-called cranking procedure, which is justified by the variational point of view [1]. Recently, we have shown [2] that indeed the calculated moment of inertia is considerably increased if the projection is performed from the cranked mean-field state with very small cranking frequency. Moreover, the resultant spectrum is independent of actual values of the frequency if it is small enough [2]: We call this procedure "infinitesimal cranking." In our previous studies the self-consistent mean-field state before the cranking is either axially symmetric [2] or tetrahedrally symmetric [3,4], so that the direction of cranking axis does not matter; there is only one rotational axis for the quantum mechanical axially symmetric system, and the tetrahedral deformation is "spherical" in the sense that all rotational axes are equivalent, which is also confirmed numerically [3]. In the present work we consider the case of the triaxial deformation, where one can crank the mean-field state around three independent rotational axes. We study the effects of infinitesimal cranking around three principal axes on the spectrum of triaxially deformed nucleus obtained by the angular-momentum-projection method.

The second purpose of the present investigation is the description of the $\gamma$ vibration by the angular-momentum-projection method. The motivation emerged from the precedent analysis by the so-called triaxial projected shell-model approach [5,6]: It is concluded that rather large triaxial deformation of the mean-field is necessary to reproduce the very low-lying nature of the $\gamma$ vibration; see also Refs. [7,8] for studies with the axial projected shell model. The $\gamma$ vibration is the most well recognized collective vibration in atomic nuclei [1,9,10]. In the rare-earth region the ground state is believed to be axially deformed according to the mean-field calculations by, e.g., the Strutinsky shell correction method and/or the Skyrme HFB method, and the $\gamma$ vibration is interpreted as a surface vibration that dynamically breaks the axial symmetry. In fact, the $\gamma$ vibration has been studied by the random phase approximation (RPA) calculation with the schematic $QQ$-type interaction based on the axially symmetric vacuum state [11], although the strong anharmonicity for two-phonon states exists; see, e.g., Refs. [12–15] and references therein. However, there is a long history on the interpretation of the $\gamma$ vibration; by employing the asymmetric (triaxial) rotor model [16] it was discussed in the early days that its low-lying nature indicates the considerable triaxial deformation, although it is very difficult to draw a definite conclusion from the existing experimental data. Therefore, the analysis by the triaxial projected shell model [5,6] revived the old problem, whether the nucleus in the rare-earth region is axially symmetric or triaxially deformed. It is worthwhile mentioning that in the triaxially deformed case the high-spin part of the multiple rotational bands based on the excitations of the $\gamma$ vibration is interpreted as the wobbling-phonon bands [10]. We briefly discuss also this interesting issue of the relation between the multiple $\gamma$ bands and the wobbling band.

As for the proper treatment of the triaxial degree of freedom, we use the configuration-mixing, or the generator coordinate method (GCM) [1], on top of the angular-momentum-projection. One of the great merits of this microscopic approach is that not only the energy spectrum but also the transition probability can be calculated fully quantum

 

mechanically without any ambiguity. It is known that the $E2$ transition probability between the ground state and the $\gamma$ vibrational state is overestimated in the RPA approach with schematic interaction by a factor 3–4 in the rare-earth region if the Nilsson potential is used as a mean field [12]; the situation is improved if the Woods-Saxon potential is used instead, but the $B(E2)$ is still overestimated by a factor 2–3 [17]. It is shown that this problem is greatly improved in our angular-momentum-projected configuration-mixing approach. We employ the Gogny D1S force [18] as an effective interaction and select the nucleus $^{164}$Er as a typical example of rare-earth nuclei. We present and discuss our results in comparison with experimental data and with the previous pioneering works [5]. The paper is organized as follows. The basic formulation of the method employed is briefly outlined in Sec. II. The results of the numerical calculations are presented in Sec. III, where the effects of the triaxial deformation and the infinitesimal cranking are discussed. In the final section, Sec. IV, we give summary of the present work and further discussion.

## II. THEORETICAL FRAMEWORK

### A. Angular-momentum-projected configuration mixing

The calculational method we employ is the standard one [1], and the wave function $|\Psi^I_{M,\alpha}\rangle$, where $\alpha$ specifies the quantum numbers other than the angular momentum $(IM)$, is obtained in the form

$$\left|\Psi^I_{M,\alpha}\right\rangle = \sum_{Kn} g^I_{Kn,\alpha}\, P^I_{MK} |\Phi_n\rangle, \tag{1}$$

where the operator $P^I_{MK}$ is the angular-momentum projector and $|\Phi_n\rangle$ $(n = 1,2,\ldots)$ are the mean-field states, which are specified in more detail in the following. The amplitude $g^I_{Kn,\alpha}$ is determined by the so-called Hill-Wheeler equation,

$$\sum_{K'n'} \mathcal{H}^I_{K,K'n'}\, g^I_{K'n',\alpha} = E^I_\alpha \sum_{K'n'} \mathcal{N}^I_{Kn,K'n'}\, g^I_{K'n',\alpha}, \tag{2}$$

with definitions of the Hamiltonian and norm kernels,

$$\begin{Bmatrix} \mathcal{H}^I_{Kn,K'n'} \\ \mathcal{N}^I_{Kn,K'n'} \end{Bmatrix} = \langle\Phi_n| \begin{Bmatrix} H \\ 1 \end{Bmatrix} P^I_{KK'} |\Phi_{n'}\rangle; \tag{3}$$

see, e.g., Ref. [1] for more details. We do not perform the number projection in the present work and treat the number conservation approximately by replacing $H \to H - \lambda_\nu(N - N_0) - \lambda_\pi(Z - Z_0)$, where $N_0$ and $Z_0$ are the neutron and proton numbers to be fixed. As for the neutron and proton chemical potentials $\lambda_\nu$ and $\lambda_\pi$, we use those obtained for the HFB ground state.

A set of the mean-field states, $|\Phi_n\rangle$ $(n = 1,2,\ldots)$, are calculated by the constrained HFB method with the quadrupole operators, $Q_{20}$ and $Q_{22}$ in $Q_{2m} \equiv r^2 Y_{2m}$, with $Y_{lm}$ being the spherical harmonics, as constraints. In place of the HFB expectation values, $\langle Q_{20}\rangle$ and $\langle Q_{22}\rangle$, we actually constrain two quantities $(Q,\gamma)$ defined by

$$Q \equiv \sqrt{\langle Q_{20}\rangle^2 + 2\langle Q_{22}\rangle^2}, \quad \gamma \equiv -\tan^{-1}\left(\frac{\sqrt{2}\langle Q_{22}\rangle}{\langle Q_{20}\rangle}\right), \tag{4}$$

which correspond to the quadrupole deformation parameters $(\beta_2,\gamma)$ with $\beta_2 = \frac{4\pi}{5} Q/(A\langle r^2\rangle)$ (note the Lund convention for the sign of $\gamma$). We employ the augmented Lagrangian method in Ref. [19] to achieve strict fulfillment of the constraints $(Q,\gamma)$ for arbitrarily desired values. In the present work, we mainly keep the magnitude of the quadrupole deformation $Q$ as that of the ground state and vary only the value of $\gamma$. Then the projected wave function is obtained as a function of $\gamma$,

$$\left|\Psi^I_{M,\alpha}(\gamma)\right\rangle = \sum_K g^I_{K,\alpha}(\gamma)\, P^I_{MK} |\Phi(\gamma)\rangle. \tag{5}$$

Instead of the amplitude $g^I_{K,\alpha}(\gamma)$ in Eq. (5), the properly normalized amplitude [1] is necessary in some cases,

$$f^I_{K,\alpha}(\gamma) = \sum_{K'} (\sqrt{\mathcal{N}^I})_{K,K'}\, g^I_{K',\alpha}(\gamma), \tag{6}$$

where the quantity $\sqrt{\mathcal{N}^I}$ denotes the square-root matrix of the norm kernel.

The triaxial deformation should be finally treated dynamically. This is done by the configuration-mixing or the generator coordinate method (GCM) with respect to the triaxiality $\gamma$. Thus, the wave function is obtained by

$$\left|\Psi^I_{M,\alpha}\right\rangle = \int d\gamma \sum_K g^I_{K,\alpha}(\gamma)\, P^I_{MK} |\Phi(\gamma)\rangle \tag{7}$$

in the continuum limit of the variable $\gamma$ under the fixed value of $Q$. In this case the norm kernel is expressed like $\mathcal{N}^I_{K,K'}(\gamma,\gamma')$ and the properly normalized amplitude is calculated by

$$f^I_{K,\alpha}(\gamma) = \int d\gamma' \sum_{K'} (\sqrt{\mathcal{N}^I})_{K,K'}(\gamma,\gamma')\, g^I_{K',\alpha}(\gamma'), \tag{8}$$

with which the probability distribution of the eigenstate $|\Psi^I_{M,\alpha}\rangle$ with respect to the $\gamma$ coordinate,

$$p^I_\alpha(\gamma) = \sum_K \left|f^I_{K,\alpha}(\gamma)\right|^2, \tag{9}$$

can be studied.

We have recently developed an efficient method to perform the angular-momentum-projection calculation [2], and it is successfully applied to the study of the nuclear tetrahedral symmetry [3,4]: The method is fully employed also in the present work. The same configuration-mixing method has been also utilized for the study of the rotational motion in Ref. [20], where the generator coordinate is chosen to be the rotational frequency $\omega_{\rm rot}$ instead of the triaxiality parameter $\gamma$. See Refs. [2,4,20] for more details of our method of calculation.

### B. Cranking procedure with infinitesimal rotational frequencies

As has been stressed in Refs. [2,3,20], it is very important to include the time-odd components in the mean-field wave function $|\Phi(\gamma)\rangle$, from which the angular-momentum projection is performed, to properly describe the moment of inertia of rotational band. This can be achieved by the cranking procedure with infinitesimally small rotational frequencies. Namely, considering that we are dealing with the triaxial deformation, the "3D cranked Hamiltonian" with the angular

momentum operators $J \equiv (J_x, J_y, J_z)$,

$$H' \equiv H - \omega \cdot J = H - \omega_x J_x - \omega_y J_y - \omega_z J_z, \tag{10}$$

is used in the constrained HFB calculation. If the cranking axis specified by the direction of the frequency vector $\omega$ does not coincide with one of the inertia axes, i.e., in the case of the tilted-axis cranking, the intrinsic coordinate frame rotates during the iterations of self-consistent calculation. Therefore, we require the following additional principal-axis constraints according to Ref. [21],

$$\langle Q_{21} \rangle = \langle Q_{2-1} \rangle = 0 \quad \text{and} \quad \langle Q_{22} \rangle = \langle Q_{2-2} \rangle. \tag{11}$$

In fact, the quantity $\langle Q_{22} \rangle$ takes real value by the second condition in Eq. (11) and then Eq. (4) is well-defined. In the present work we only consider the case of infinitesimal cranking, but the large rotational frequencies with the tilted-axis cranking can be applied to study various high-spin phenomena; see, e.g., Ref. [22].

In this section we discuss what kind of time-odd components are included by the 3D cranking in Eq. (10) and show that the result of angular-momentum projection depends on the particular choice of neither the cranking frequency nor the cranking axis as long as the values of frequencies $\omega = (\omega_x, \omega_y, \omega_z)$ are small. Therefore, there is no ambiguity in this infinitesimal cranking procedure. The content was partly discussed in relation to the zero frequency limit in Sec. III C of Ref. [2], but the independence of the result was not fully explained. Moreover, the case considered was somewhat specific; the ground state before the cranking is axially symmetric and its wave function has only $K = 0$ components. Here we consider more general cases for even-even nuclei, where the ground mean-field state before the cranking is time-reversal invariant and has the $D_2$-symmetry belonging to the totally symmetric $(r_x, r_y, r_z) = (+1, +1, +1)$ representation [10]. Here $r_i$ $(i = x, y, z)$ is the quantum number of the $i$ signature, i.e., the $\pi$ rotation around the $i$ axis, and $r_x r_y r_z = +1$. The classification of the projected states according to the $y$ signature quantum number is convenient for the projection calculation using the usual rotation operator $R(\alpha, \beta, \gamma) = e^{i\gamma J_z} e^{i\beta J_y} e^{i\alpha J_z}$. In Ref. [2] the $x$ signature is employed instead but the conclusion does not change. For the notational simplicity we neglect the irrelevant configuration-mixing in this section but the extension is trivial. Then the wave function in Eq. (1) is written in the $y$-signature-classified way [10] as

$$\left|\Psi^I_{M,\alpha}\right\rangle = \sum_{K \geqslant 0} \left( \tilde{g}^I_{K,\alpha}\, \tilde{P}^I_{MK} + \tilde{g}^I_{\bar{K},\alpha}\, \tilde{P}^I_{M\bar{K}} \right) |\Phi\rangle, \tag{12}$$

where the amplitudes $(\tilde{g}^I_{K,\alpha}, \tilde{g}^I_{\bar{K},\alpha};\ K \geqslant 0)$ are defined by

$$\begin{aligned} \tilde{g}^I_{K,\alpha} &\equiv \frac{1}{\sqrt{2(1+\delta_{K0})}} \left[ g^I_{K,\alpha} + (-1)^{I+K} g^I_{-K,\alpha} \right] \quad \text{for } r_y = +1, \\ \tilde{g}^I_{\bar{K},\alpha} &\equiv \frac{1}{\sqrt{2(1+\delta_{K0})}} \left[ g^I_{K,\alpha} - (-1)^{I+K} g^I_{-K,\alpha} \right] \quad \text{for } r_y = -1, \end{aligned} \tag{13}$$

and the modified projectors $(\tilde{P}^I_{MK}, \tilde{P}^I_{M\bar{K}})$ are defined in the same way. For the noncranked mean-field state $|\Phi\rangle$, which is totally $D_2$ symmetric, only the components compatible with the representation $(r_x, r_y, r_z) = (+1, +1, +1)$ survive;

$$\left|\Psi^I_{M,\alpha}\right\rangle = \sum_{K = \text{even} \geqslant 0} \tilde{g}^I_{K,\alpha}\, \tilde{P}^I_{MK} |\Phi\rangle. \tag{14}$$

If the cranking frequency vector $\omega$ is small, the first-order perturbation theory can be applied for the self-consistent mean-field state $|\Phi(\omega)\rangle$ calculated with the Routhian in Eq. (10),

$$|\Phi(\omega)\rangle \approx |\Phi\rangle + \omega \cdot C |\Phi\rangle, \tag{15}$$

where $C = (C_x, C_y, C_z)$ are one-body operators defined with respect to $|\Phi\rangle$ and related to the so-called angle operators canonically conjugate to $(J_x, J_y, J_z)$ in the RPA [1]. If the total Hamiltonian in Eq. (10) were approximated by the mean-field Hamiltonian neglecting the effect of the residual interaction, then the operator $C_i$ $(i = x, y, z)$ could be written in a simple well-known form,

$$H \approx h = \sum_\alpha E_\alpha a^\dagger_\alpha a_\alpha \Rightarrow C_i \approx \sum_{\alpha > \beta} \left[ \frac{(J_i)_{\alpha\beta}}{E_\alpha + E_\beta} a^\dagger_\alpha a^\dagger_\beta - \text{H.c.} \right], \tag{16}$$

where $(a^\dagger_\alpha, a_\alpha)$ are the creation and annihilation operators of the quasiparticle, $E_\alpha$ is the quasiparticle energy, and $(J_i)_{\alpha\beta}$ is the matrix element of the operator $J_i$ with respect to the quasiparticle states. Note that the operators $(C_x, C_y, C_z)$ have the same $D_2$-symmetry property as $(J_x, J_y, J_z)$ for the totally $D_2$-symmetric state $|\Phi\rangle$. Taking into account the fact that the operators $J_x$, $J_y$, and $J_z$ belong to the representation $(r_x, r_y, r_z) = (+1, -1, -1)$, $(-1, +1, -1)$, and $(-1, -1, +1)$, respectively, the projected state from the cranked mean-field state (15) can be classified into the four terms:

$$\begin{aligned} \left|\Psi^I_{M,\alpha}\right\rangle &= \sum_{K \geqslant 0} \left( \tilde{g}^I_{K,\alpha}\, \tilde{P}^I_{MK} + \tilde{g}^I_{\bar{K},\alpha}\, \tilde{P}^I_{M\bar{K}} \right) |\Phi(\omega)\rangle \\ &\approx \sum_{K = \text{even} \geqslant 0} \tilde{g}^I_{K,\alpha}\, \tilde{P}^I_{MK} |\Phi\rangle \\ &\quad + \sum_{K = \text{odd} > 0} \omega_x \tilde{g}^I_{\bar{K},\alpha}\, \tilde{P}^I_{M\bar{K}} C_x |\Phi\rangle \\ &\quad + \sum_{K = \text{odd} > 0} \omega_y \tilde{g}^I_{K,\alpha}\, \tilde{P}^I_{MK} C_y |\Phi\rangle \\ &\quad + \sum_{K = \text{even} \geqslant 0} \omega_z \tilde{g}^I_{\bar{K},\alpha}\, \tilde{P}^I_{M\bar{K}} C_z |\Phi\rangle. \end{aligned} \tag{17}$$

Thus, each component of the 3D cranking procedure in Eq. (10) induces different time-odd terms that are classified according to the $D_2$-symmetry quantum numbers $(r_x, r_y, r_z)$. Moreover, three frequencies $(\omega_x, \omega_y, \omega_z)$ appear in combination with the amplitudes $g^I_{K\alpha}$, and so the change of frequencies can be absorbed into the change of the amplitudes when the Hill-Wheeler equation (2) is solved (even the sign of the frequencies does not matter). Namely, it has been shown that the result of the angular-momentum projection is independent of the infinitesimally small values of frequencies $(\omega_x, \omega_y, \omega_z)$ within the first-order perturbation theory.

In the case of axial symmetry around the $z$ axis the operator $C_z$ vanishes and the remaining two terms $C_x|\Phi\rangle$ and $C_y|\Phi\rangle$ give the same contribution (the $x$ and $y$ axes are equivalent).

Therefore, there is only one extra term instead of three included by the infinitesimal cranking.

In Ref. [2] it was found that the spectrum obtained by projection from the cranked HFB state with vanishingly small frequency is different from the one obtained by projection from the noncranked HFB state. Namely, the projected spectrum is discontinuous in the zero frequency limit. The reason is quite obvious from the argument above; the projected state from the cranked HFB state (17) is always different from the one projected from the noncranked HFB state (14) even if the frequencies are vanishingly small but nonzero.

## III. RESULTS OF NUMERICAL CALCULATION

In the present work we adopt the finite-range Gogny force with the D1S parametrization [18] as an effective interaction throughout; the treatment of the Gogny force is the same as in Ref. [20]. Therefore, there is no ambiguity about the Hamiltonian. We apply the theoretical framework of the previous section to a typical rare-earth nuclei, $^{164}$Er, where the low-lying $\gamma$ vibrational $2^+_\gamma$ state is observed at the excitation energy, 0.860 MeV. The constrained HFB Hamiltonian is diagonalized on the basis of the isotropic harmonic oscillator potential with the frequency $\hbar\omega = 41/A^{1/3}$ MeV, and the same basis is utilized in the subsequent angular-momentum-projection calculation. The size of the basis states is controlled by the oscillator quantum numbers; all the states with $n_x + n_y + n_z \leqslant N_{\rm osc}^{\rm max}$ are included. $N_{\rm osc}^{\rm max} = 10$ is used in the following calculations. We do not intend to discuss very high-spin states and we take $I_{\rm max} = 40$ and $K_{\rm max} = 30$. The number of mesh points $(N_\alpha, N_\beta, N_\gamma)$ for the Euler angles $\Omega = (\alpha,\beta,\gamma)$ utilized in the numerical integration of the angular-momentum-projection operator are chosen to be $N_\alpha = N_\gamma = 62$ and $N_\beta = 82$, which is checked to be enough even for large triaxial deformations. The canonical basis cutoff parameter is taken to be $10^{-6}$ as in the all previous calculations, and the norm cutoff parameter in the configuration-mixing (GCM) calculation is taken to be $10^{-10}$. As for the values of frequencies $\omega \equiv (\omega_x,\omega_y,\omega_z)$ in Eq. (10) for the infinitesimal cranking, appropriately small values should be chosen; it should be small enough for the first-order perturbation theory to be valid, while it should not be too small so that the relative magnitude of the induced time-odd components are well above the numerical accuracy. We use 10 keV/$\hbar$ for the value of the infinitesimal frequencies, which is small enough to guarantee the independence of the result for excitation spectrum within about 1 keV for low-lying states.

Calculated mean-field parameters of the ground state of $^{164}$Er are $Q = 5.644$ b and $\beta_2 = 0.316$ for the quadrupole deformation, which is axially symmetric, and $\bar{\Delta}_\nu = 0.846$ MeV and $\bar{\Delta}_\pi = 0.859$ MeV for the neutron and proton average pairing gaps, respectively. Here $\bar{\Delta}$ is defined by $\bar{\Delta} \equiv -(\sum_{a>b} \Delta_{ab}\kappa^*_{ab})/(\sum_{a>b} \kappa^*_{ab})$, where $\kappa_{ab}$ is the abnormal density matrix (the pairing tensor) and $\Delta_{ab}$ is the matrix element of the pairing potential [1]. These values are slightly different from those—$\beta_2 = 0.311$, $\bar{\Delta}_\nu = 0.874$ MeV, and $\bar{\Delta}_\pi = 0.906$ MeV—in Ref. [20] because of the different size of the model space ($N_{\rm osc}^{\rm max} = 12$ in Ref. [20]).

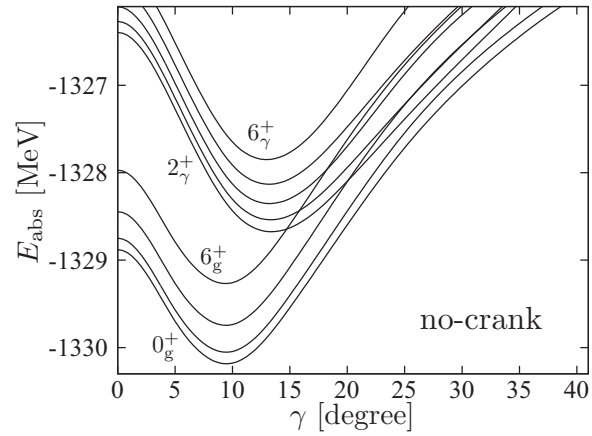


FIG. 1. Absolute energy curves as functions of the triaxial deformation parameter $\gamma$ calculated by the angular-momentum projection from the noncranked HFB ground state in $^{164}$Er. Those for the $0^+$, $2^+$, $4^+$, and $6^+$ states of the g band and for the $2^+$, $3^+$, $4^+$, $5^+$, and $6^+$ states of the $\gamma$ band are included.

### A. Effect of triaxial deformation

There is no low-lying second $2^+$ state below 2.5 MeV if the angular-momentum-projection calculation is performed from the axially symmetric HFB state without cranking. This is because the axially symmetric HFB state (without cranking) has only $K = 0$ components of the wave function; the $|K| = 2$ components are necessary to have low excitation energy for the second $2^+$ state, which is $|K| = 2$ mode, while the first $2^+$ state is $K = 0$ mode. One way to obtain the second $2^+$ state is to construct a coherent linear combination of many $|K| = 2$ two quasiparticle states, which is the way taken by the RPA method [1]. Another easiest way is to include the $|K| = 2$ components into the HFB state, from which the projection is performed, by explicitly breaking the axial symmetry. This can be done for the quadrupole deformation by requiring the finite $\gamma$ deformation with the constraint field $-\lambda_{22}(Q_{22} + Q_{2-2})$, where the $c$ number $\lambda_{22}$ is the Lagrange multiplier; apparently it induces $|K| = 2$ (and $= 4,6,\ldots$) components in the ground-state wave function. In this section we consider the effect neither of the infinitesimal cranking nor of the configuration mixing, which is investigated in the following sections.

In the present work, we restrict, without loss of generality, the triaxial deformation in the $0 \leqslant \gamma \leqslant 60^\circ$ sector with the definition in Eq. (4). Namely, the lengths of inertia axes satisfy

$$\left\langle \sum_{a=1}^{A} (x^2)_a \right\rangle \leqslant \left\langle \sum_{a=1}^{A} (y^2)_a \right\rangle \leqslant \left\langle \sum_{a=1}^{A} (z^2)_a \right\rangle, \qquad (18)$$

where the expectation values are taken with respect to the HFB state and the first equality holds at $\gamma = 0^\circ$ and the second at $\gamma = 60^\circ$.

First of all, the calculated energies are shown as functions of the triaxiality parameter $\gamma$ in Fig. 1; we include those of the $0^+$, $2^+$, $4^+$ and $6^+$ states in the ground-state band (g band), and of the $2^+$, $3^+$, $4^+$, $5^+$, and $6^+$ states interpreted as the members of the $\gamma$ vibrational band ($\gamma$ band), which are obtained by the angular-momentum-projection from a single noncranked HFB state with triaxiality $\gamma$ as in Eq. (5). The actual calculation

is performed for ten $\gamma$ values, $\gamma = 1^\circ, 5^\circ, 10^\circ, \ldots, 40^\circ$, and $45^\circ$. As in the case of the time-odd components induced by the cranking term, the $|K| \neq 0$ components induced by the triaxial deformation make the spectrum discontinuous at $\gamma = 0$. The spectrum obtained by the projection from the axially symmetric HFB state is different from the one obtained from the HFB state with vanishingly small but nonzero triaxial deformation. We adopt $\gamma = 1^\circ$ as a vanishingly small $\gamma$. Utilizing the symmetry of energy $E(\gamma) = E(-\gamma)$, the data are extended a few points to the negative values, $\gamma = -10^\circ, -5^\circ, -1^\circ, 1^\circ, 5^\circ, 10^\circ, \ldots$, and then continuous curves are generated by the cubic-spline interpolation to make Fig. 1. Therefore, the data plotted at $\gamma = 0$ in the figure are not those obtained by setting $\gamma = 0$ but the limiting values as $\gamma \to 0$. As mentioned in Sec. II A, the magnitude of the quadrupole moment $Q$ in Eq. (4) is kept at its ground-state value in the calculation. The deformation parameter $\beta_2$ slightly changes as a function of $\gamma$ because the mean-square radius $\langle r^2 \rangle$ depends slightly on the triaxiality; the amount of change in $\beta_2$ is small, within 2%, however. One can see that the ground-state energy gains about 1.2 MeV by the angular-momentum projection at the finite triaxial deformation of about $\gamma \approx 9.7^\circ$, even if the minimum of the HFB energy is axially symmetric. This is well known for the angular-momentum projection [23,24]; breaking the symmetry always introduces new degrees of freedom and the associated correlation energy for its recovery quite often defeats the mean-field energy. All curves for members of the g band take minima at similar values, $\gamma \approx 9.7^\circ$. Therefore, we can say that the members of the g band have almost the same deformation. The same is true for members of the $\gamma$ band, although the $\gamma$ values at minima, $\gamma \approx 13.6^\circ$, are slightly larger than those of the g-band members.

Figure 2 shows the excitation energies as functions of the triaxiality parameter $\gamma$ for the $2^+$, $4^+$, and $6^+$ states in the g band and of the $2^+$, $3^+$, $4^+$, $5^+$, and $6^+$ states in the $\gamma$ band. The same interpolation technique used to draw Fig. 1 is used to draw Fig. 2. This result of the $\gamma$ dependence can be compared with that of the asymmetric rotor model with the irrotational moments of inertia in Ref. [16]; see, e.g., Ref. [9] for a more complete figure of the spectrum. Note that only the $\gamma$ dependence is meaningful for this macroscopic rotor model. The similarity is apparent: The excitation energies of the members of the $\gamma$ band rapidly decrease as triaxiality increases in the range $5^\circ \lesssim \gamma \lesssim 20^\circ$ and the $2^+_\gamma$ energy crosses the $6^+_g$ energy at $\gamma \approx 15^\circ$. Moreover, small bulges are observed at around $\gamma \approx 30^\circ$ in the $4^+_\gamma$ and $6^+_\gamma$ curves, which makes the energies of the even-spin members higher than those of the odd-spin members, leading to the characteristic band structure of the wobbling band. However, there are marked differences: The spectrum is symmetric with respect to the $\gamma = 30^\circ$ axis in the triaxial rotor model with the irrotational inertia but not exactly symmetric in our microscopic angular-momentum-projection calculation, and the bulges around $\gamma \approx 30^\circ$ in the $4^+_\gamma$ and $6^+_\gamma$ curves are not so pronounced as in the case of the rotor model. The most striking difference is that the second $2^+$ state appears at around 2.5 MeV even with the small triaxiality $\gamma \approx 1^\circ$–$5^\circ$ in the microscopic calculation; however, the collectivity is not as high as experimentally observed. At $\gamma \approx 9.7^\circ$, where the ground-state energy takes

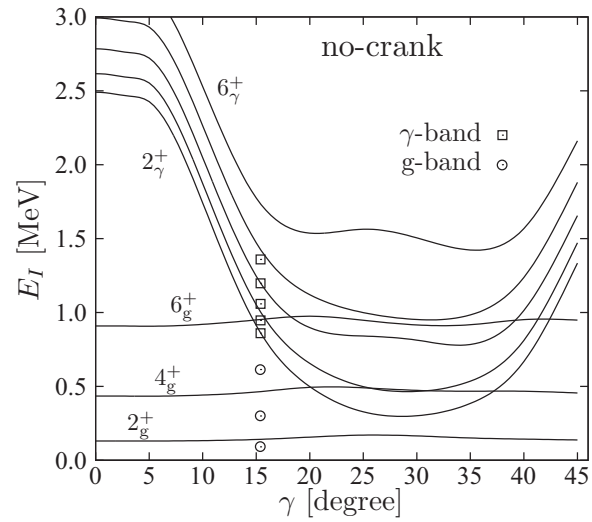


FIG. 2. Excitation energy curves as functions of the triaxial deformation parameter $\gamma$ calculated by the angular-momentum projection from the noncranked HFB ground state in $^{164}$Er. Those for the $2^+$, $4^+$, and $6^+$ states of the g band and for the $2^+$, $3^+$, $4^+$, $5^+$, and $6^+$ states of the $\gamma$ band are included. Experimental data are also shown by symbols, open circles and squares, at $\gamma = 15.4^\circ$, where the calculated excitation energy of $2^+_\gamma$ coincides with the experimental one.

minimum (cf. Fig. 1), the excitation energy of the second $2^+$ state is about 1.9 MeV, while at $\gamma \approx 13.6^\circ$, where the absolute energies of members of the $\gamma$ band take minima, it is about 1.1 MeV. Compared with the experimental $\gamma$ vibrational energy, 0.860 MeV, the former value is considerably larger while the latter value is rather close.

The $\gamma$ value, at which the calculated $2^+_\gamma$ energy agrees with the observed one, is $\gamma \approx 15.4^\circ$; the experimental excitation energies are included in Fig. 2 at this value. We show in Fig. 3 the calculated spectrum with this value, $\gamma = 15.4^\circ$, in comparison with experimental data. Interestingly, the multiple band structure, the one-, two-, and three-phonon excited bands

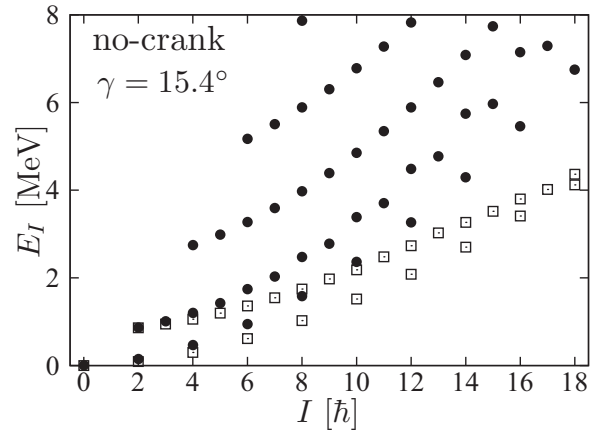


FIG. 3. Energy spectrum calculated by the angular-momentum projection from the noncranked HFB state at $\gamma = 15.4^\circ$ in $^{164}$Er. The experimental data for the g band and the $\gamma$ band are included as open squares.

starting from $I = 2_2^+$, $4_3^+$, and $6_4^+$ states, respectively, are clearly seen with strong anharmonicity; the excitation energy of the two(three)-phonon state, $4_3^+(6_4^+)$, is considerably larger than the value which is two(three) times that of the one-phonon state, $2_2^+$. Moreover, the signature splitting is observed in the high-spin part of the one-phonon band; i.e., the odd-spin members are lower in energy than the even-spin member, which is characteristic for the wobbling excitations. This behavior is more strongly observed at larger values of the triaxiality parameter $\gamma$; cf. the next section. However, the agreement of the calculated energies with the experimental data is not satisfactory. The moments of inertia of both the g band and the $\gamma$ band are too small; i.e., the energy spacings of the neighboring states in both bands are too large. We need some improvements to obtain better agreement, which is considered in the next section.

A similar result has been reported by the triaxial projected shell model; cf. Fig. 1 of Ref. [5], which can be compared with our result in Fig. 2. However, one should be careful about the difference of the way of presentation. In the works of the triaxial projected shell model, a deformed quadrupole potential is utilized,

$$-\frac{2}{3}\sqrt{\frac{4\pi}{5}}\frac{\hbar\omega_0}{b_0^2}\left[\epsilon\, Q_{20} + \epsilon'\frac{1}{\sqrt{2}}(Q_{22} + Q_{2-2})\right], \qquad (19)$$

where the quantity $b_0$ is the oscillator length associated with the oscillator frequency $\omega_0$. In Ref. [5] the excitation energies are shown as functions of the parameter $\epsilon'$ with keeping another parameter $\epsilon$ at the ground-state value. Our $\beta_2$ and $\gamma$ deformation parameters roughly correspond to $\sqrt{\frac{16\pi}{45}}\sqrt{\epsilon^2+\epsilon'^2}$ and $-\tan(\epsilon'/\epsilon)$, respectively. Therefore, apart from the sign of $\gamma$, which is irrelevant in the present context, the $\beta_2$ value is increased when increasing $\epsilon'$ in the calculation of Ref. [5], while $\beta_2$ is kept constant within 2% in our calculation. At first sight, the result of Ref. [5] is very similar to ours, e.g., the excitation energies of members of the $\gamma$ band quickly decrease as functions of the parameter $\epsilon'$, although the agreement with the experimental data is much better than ours when the value of $\epsilon'$ is appropriately chosen. However, the value of triaxial deformation, at which the calculated spectrum agrees with the experimental one, seems quite different in Ref. [5]; for the $^{164}$Er nucleus, $\epsilon = 0.258$ and $\epsilon' = 0.14$, which correspond to $\beta_2 \approx 0.310$ and $|\gamma| \approx 28.5^\circ$. The value of $\beta_2$ is very similar to ours, $\beta_2 \approx 0.316$, while that of $\gamma$ is much larger than ours $\gamma \approx 15.4^\circ$.

On this difference, however, one has to be careful about the definition of the triaxiality parameter: The one utilized in Ref. [5] is defined with respect to the shape of the single-particle potential, $\gamma_{\rm pot}$, while the one utilized in the present work is defined with respect to the shape of the density distribution, $\gamma_{\rm den}$. It has been discussed in Refs. [25,26] that the difference between these two parameters $\gamma_{\rm pot}$ and $\gamma_{\rm den}$ is rather large for well-deformed nuclei. Note that the $\gamma_{\rm pot}$ defined for the Nilsson potential is still different from the one utilized in Eq. (19), $\gamma_{\rm pot} \equiv -\tan(\epsilon'/\epsilon)$. For the harmonic oscillator potential model with the self-consistent deformation condition [10], the transformation between the deformation parameters in these different definitions can be done easily

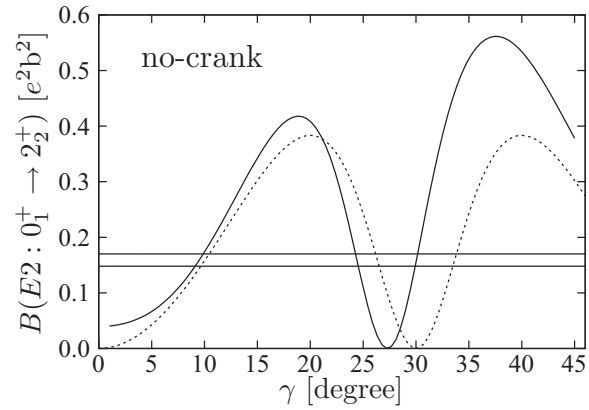


FIG. 4. $E2$ transition probability from the ground state to the second $2^+$ state as a function of the triaxial deformation parameter $\gamma$, which is calculated by the angular-momentum projection from the noncranked HFB state in $^{164}$Er (solid curve). The dotted curve is the prediction of the asymmetric rotor model [16] in Eq. (20) with $B = 5.723$ ($e^2$b$^2$). The experimentally measured values [27], 0.148 and 0.170 ($e^2$b$^2$), are shown by two horizontal lines, which are deduced from two different types of reactions.

(see Appendix of Ref. [26]); the values $\beta_{\rm pot} = 0.310$ and $\gamma_{\rm pot} = 28.5^\circ$ correspond to $\beta_{\rm den} = 0.334$ and $\gamma_{\rm den} = 17.6^\circ$. In this way the triaxiality $\gamma_{\rm den}$ is not very different from our value $15.4^\circ$, although $\beta_2$ is a little bit larger. Thus, taking these differences into account, the results of Ref. [5] and ours are rather consistent with each other. However, the expected triaxial deformation $\gamma_{\rm den} \approx 15^\circ$–$18^\circ$ is too large if the $E2$ transition probability between the g band and the $\gamma$ band is investigated.

Thus, we show in Fig. 4 the $B(E2)$ value for the transition from the $0^+$ ground state to the second $2^+$ state as a function of $\gamma$ calculated by the angular-momentum projection from the noncranked HFB state. Note that we do not use any kind of effective charge because the contributions of all nucleon are included. In the figure the result of the asymmetric rotor model with the irrotational inertia [16],

$$B(E2: 0_1^+ \to 2_2^+)_{\rm AR} = \frac{B}{2}\left[1 - \frac{3 - 2\sin^2(3\gamma)}{\sqrt{9 - 8\sin^2(3\gamma)}}\right](e^2\mathrm{b}^2), \qquad (20)$$

is also included as the dotted curve, where $B$ is the in-band transition probability for the g band, $B(E2: 0_1^+ \to 2_1^+)$ at $\gamma = 0$. The calculated value is $B = 5.723$ ($e^2$b$^2$), which well corresponds to the experimentally measured value, 5.81 ($e^2$b$^2$). As is well known, this $B(E2: 0_1^+ \to 2_2^+)$ of the rotor model rapidly increases with increasing the triaxiality, turns to decrease at $\gamma \approx 20^\circ$, and vanishes at $\gamma = 30^\circ$; the $\gamma$ dependence is symmetric about $\gamma = 30^\circ$ axis. The rotor model wave function is represented with the Wigner-$D$ function as $\sum_K f^I_{K,\alpha}\mathcal{D}^I_{MK}(\Omega)$, where the amplitudes $f^I_{K,\alpha}$ correspond to those properly normalized in Eq. (6), and the transition amplitude is evaluated as

$$\begin{aligned}\langle 2_2^+||Q_2^{(E)}||0_1^+\rangle &\propto f^{2_2^+}_{K=0}\langle Q_{20}^{(E)}\rangle + 2f^{2_2^+}_{K=2}\langle Q_{22}^{(E)}\rangle \\ &= Q^{(E)}\left(f^{2_2^+}_{K=0}\cos\gamma - 2f^{2_2^+}_{K=2}\sin\gamma\right), \qquad (21)\end{aligned}$$

where $Q^{(E)}_{2\mu}$ is the electric quadrupole operator (i.e., $e$ times the proton contribution) and it is assumed that the deformation of neutrons and protons is the same. For $\gamma < 20^\circ$ the $2^+_2$ state is almost purely $K = 2$ mode and the $K = 0$ amplitude is almost negligible; therefore, the $B(E2)$ increases as $\propto \sin^2\gamma$ as $\gamma$ increases from 0 with the electric quadrupole moment $Q^{(E)}$ being fixed. Further increasing $\gamma > 20^\circ$, however, the $K$ mixing quickly grows and the two terms in Eq. (21) tend to cancel each other; the exact cancellation occurs at $\gamma = 30^\circ$ for the rotor model with the irrotational inertia. The microscopically calculated transition amplitude approximately satisfies Eq. (21) and the resultant $B(E2)$ roughly follows the trend of the rotor model, although it is not rigorously symmetric as in the case of the excitation spectrum and vanishes at $\gamma \approx 27^\circ$. Moreover, the calculated value is considerably larger than that in the rotor model at $\gamma \gtrsim 30^\circ$. The calculated $B(E2)$ values at small triaxiality, $\gamma \approx 1^\circ$–$5^\circ$, are about four to six times the single-particle unit, which is two times the Weisskopf unit [10], $B_{\rm s.p.} = 2B_{\rm W}(E2) = 0.0107$ ($e^2$b$^2$) in $^{164}$Er. The experimentally measured value [27], 0.148 or 0.170 ($e^2$b$^2$), is about 14 to 16 times the single-particle unit and can be reproduced by the calculation with $\gamma \approx 10^\circ$. Apparently, if one employs the result with $\gamma \approx 15^\circ$–$18^\circ$, the $B(E2)$ value is overestimated by about a factor two to three as long as the calculated quadrupole moment $Q^{(E)}$ is used, which well reproduces the rotational $B(E2)$ values inside the g band assuming the axial symmetry ($\gamma = 0$) as it was demonstrated in our previous work [20].

It is worthwhile mentioning that the calculated in-band $B(E2)$ value for the g band, $B(E2: 0^+_1 \to 2^+_1)$, as a function of $\gamma$ also well coincides with the result of the asymmetric rotor model, which is obtained by changing the first sign in Eq. (20) from $-$ to $+$ [16], although the deviation is non-negligible for $\gamma \gtrsim 27^\circ$ (not shown).

### B. Effect of infinitesimal cranking

In the previous section it is found that the spectrum obtained by the angular-momentum projection from the noncranked HFB state is not very good in comparison with the experimental data. The first problem is that the moment of inertia is too small, which was already stressed in Ref. [2]. Moreover, considerable triaxial deformation, $\gamma \gtrsim 15^\circ$, is necessary to reproduce the low-lying nature of the $\gamma$ vibration, which is not justified from the energy minimization (cf. Fig. 1) and from the $B(E2: 0^+_1 \to 2^+_2)$ value; the $B(E2)$ value for such triaxial deformation, $\gamma \gtrsim 15^\circ$, is too large compared with the measured value. To achieve a better description of the rotational motion for triaxial nuclei, we here study the effect of infinitesimal cranking, which is explained in detail in Sec. II B.

In Figs. 5 and 6 we show how the spectrum changes for the triaxial deformation with $\gamma = 10^\circ$ and $\gamma = 20^\circ$, respectively, if the infinitesimally cranked HFB state is employed instead of the noncranked one for the angular-momentum-projection. As discussed in Sec. II B, there are three independent axes for cranking. The results of all seven cases in addition to the noncranked one are included in the figures; the principal-axis cranking around the $x$, $y$, and $z$ axis, and the planar tilted-axis cranking around the $xy$, $yz$, and $zx$ axes, and finally the

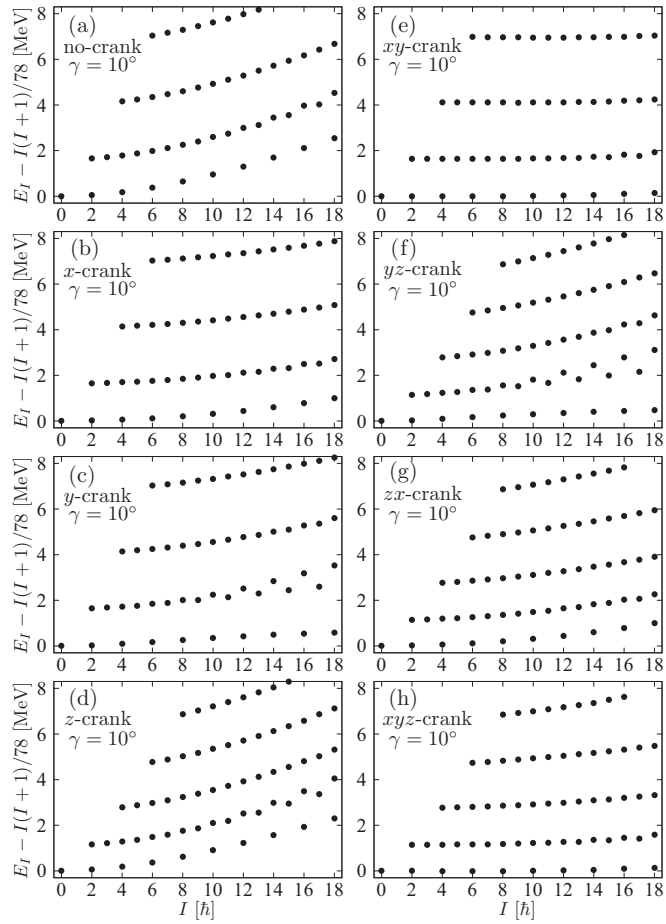


FIG. 5. Energy spectrum calculated by the angular-momentum projection from the infinitesimally cranked HFB state with triaxial deformation, $\gamma = 10^\circ$, for $^{164}$Er. The axis (axes) of cranking is (are) specified in each panel, e.g., "$xyz$ crank" means that the infinitesimal cranking is performed about all the $x$, $y$, and $z$ axes. The noncranked case is also included as panel (a).

nonplanar tilted-axis cranking around all the $xyz$ axes. To see each spectrum in more detail, the reference rotational energy, $I(I+1)/(2\mathcal{J}_0)$, is subtracted with $\mathcal{J}_0 = 39\,(\hbar^2/\text{MeV})$, which roughly corresponds to the average moment of inertia of the experimentally observed g band in $^{164}$Er. In the case of smaller triaxiality $\gamma = 10^\circ$ in Fig. 5(a), one can see nice multiple rotational bands without cranking, as discussed in Fig. 3. With the $x$- and $y$-axis cranking, Figs. 5(b) and 5(c), the slopes of the multiple bands decrease considerably, while with the $z$-axis cranking, Fig. 5(d), the relative excitation energies of excited bands from the g band decrease. It can be seen that the excitation energy of the $\gamma$ vibration is roughly 1.2 MeV if the cranking around the $z$ axis is performed, while it is about 1.7 MeV without it for $\gamma = 10^\circ$; thus, the considerable reduction of excitation energy is observed by the $z$-axis cranking. Comparing with the $x$- and $y$-axis cranking, the increase of the moment of inertia is more or less the same (or slightly larger with the $y$-axis cranking) for $\gamma = 10^\circ$, although the signature splitting of the one-phonon $\gamma$ band, i.e., the splitting between the even-$I$ and odd-$I$ members,

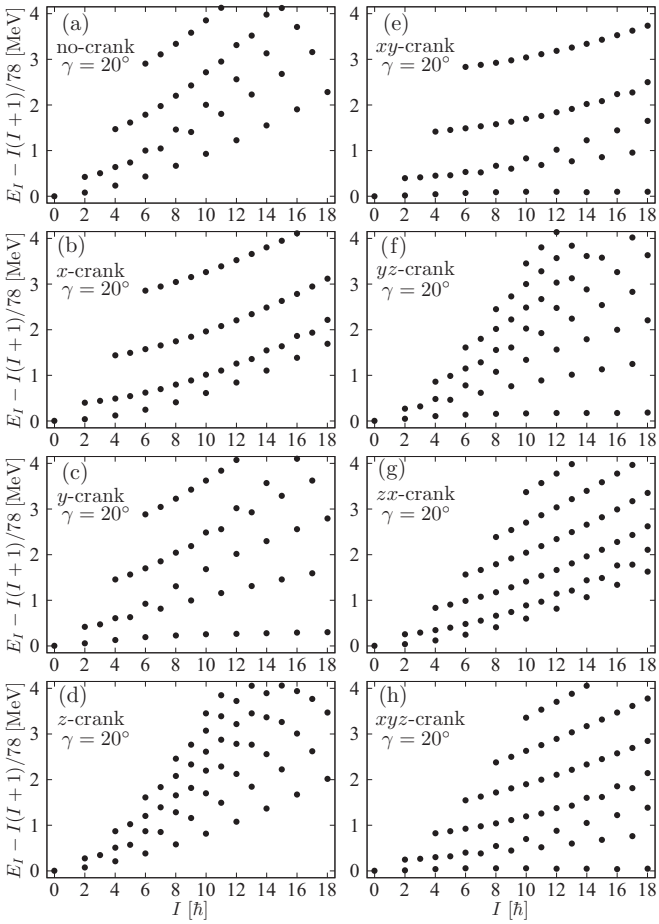


FIG. 6. Energy spectrum calculated by the angular-momentum projection from the infinitesimally cranked HFB state with triaxial deformation, $\gamma = 20°$, for $^{164}$Er. The axis (axes) of cranking is (are) specified in each panel, e.g., "$xyz$ crank" means that the infinitesimal cranking is performed about all the $x$, $y$, and $z$ axes. The noncranked case is also included as panel (a).

increases by the $y$-axis cranking, while it decreases by the $x$-axis cranking. The combination of cranking around two axes, Figs. 5(e)–5(g), gives more or less combined effects; for example, with the $xy$ cranking the increase of the moments of inertia for multiple bands is largest. The results with the $yz$ and the $zx$ cranking have similar multiple band structures, but the signature splitting is only apparent in the case of the $yz$ cranking. With the cranking around all three axes in Fig. 5(h), the largest effect is observed and all multiple rotational bands are approximately parallel and almost horizontal with smaller excitation energies than those of the noncranked case.

With larger triaxial deformation, $\gamma = 20°$, in Fig. 6, the basic trend is similar, e.g., the reduction of the excitation energy of the $\gamma$ vibration is largest with the $z$-axis cranking and the large signature splitting is induced by the $y$-axis cranking. However, considerable differences from the case with smaller triaxial deformation, $\gamma = 10°$, in Fig. 5 are observed; the signature splitting is much larger except for the cases where the $x$-axis cranking is performed without the $y$-axis cranking in Figs. 6(b) and 6(g). Generally, an increase of moments of inertia is observed for all multiple bands, but the amounts of increase are somewhat different for each band and those of the excited bands are not so large compared with the case with smaller triaxiality, $\gamma = 10°$. The only exception is the g band, which is almost horizontal, if the $y$-axis cranking is performed as is seen in Figs. 6(c), 6(e), 6(f), and 6(h); in the case of $\gamma = 20°$ the increase of inertia is largest with the $y$-axis cranking. The signature splitting is generally larger with larger triaxial deformation, as seen even in the case without cranking; compare Figs. 5(a) and 6(a). The larger signature splitting induced by the $y$- and $z$-axis cranking, [cf. Figs. 6(c), 6(d), and 6(f)] makes the band structure as if it is composed of the even-$I$ and odd-$I$ sequences alternately, which is characteristic for the wobbling rotational band. With the cranking around all three axes in Fig. 6(h), nice multiple band structure appears with the wobblinglike structure developing at higher-spin part. The relation to the wobbling band is briefly discussed in the following section.

In Table I the first and second excited $2^+$ energies obtained by the angular-momentum projection with the infinitesimal cranking around various axes are summarized for $\gamma = 10°$ and $\gamma = 20°$. The $B(E2)$ values of the transition from the ground state to the second excited $2^+$ state are also included. It is clear that the first $2^+$ state in the g band is lowered in energy by the $x$- and $y$-axis cranking, while the second $2^+$ state in the $\gamma$ band is lowered by the $z$-axis cranking, as was discussed in relation to Figs. 5 and 6. As for the $B(E2)$ value, however, it increases by the $x$-axis cranking, while it decreases by the $y$- and $z$-axis cranking; the $z$-axis cranking especially reduces the transition markedly, and the simultaneous $yz$ cranking makes the $B(E2)$ value about one-third compared with the case without cranking for the triaxiality $\gamma = 20°$. In this way, it is interesting to see that the effects of cranking around three independent axes are quite different and the different combinations of rotation axes considerably change the resultant angular-momentum-projected spectrum in the case of triaxial deformation.

From the variational point of view the cranking around all three axes gives the best results in our theoretical framework. With the infinitesimal cranking around all three axes, i.e., the $xyz$ cranking, the calculated absolute energies for members of the g band and of the $\gamma$ band are shown as functions of the triaxiality parameter $\gamma$ in Fig. 7 as in the case without cranking in Fig. 1, and the calculated excitation energies are shown in Fig. 8 as in the case without cranking in Fig. 2. The same interpolation technique is used to draw Figs. 7 and 8 as Figs. 1 and 2. Comparing these two sets of figures, the absolute $0^+$ ground-state energy is very similar, while the excitation energies of members of both the g band and the $\gamma$ band decrease considerably. This means that the moment of inertia is increased by the infinitesimal cranking on one hand, and the excitation energy of the $\gamma$ vibration is decreased on the other hand, which was already discussed in relation to Figs. 5 and 6. The value of triaxiality $\gamma$, which gives the minimum energy for the $0^+$ ground state, is about $\gamma \approx 9.7°$; it is almost the same as in the case without cranking. In contrast, the value which gives the minimum energy of the $2^+$ $\gamma$ vibrational state is about $\gamma \approx 12.2°$, which is slightly smaller than the value $\gamma \approx 13.6°$ without cranking. In Fig. 8 the experimental excitation energies are included as symbols at $\gamma = 12.8°$,

TABLE I. The excitation energies of the first and second $2^+$ states and the $B(E2: 0_1^+ \to 2_2^+)$ value calculated by the angular-momentum-projection from the infinitesimally cranked HFB state around various axes; e.g., "$xyz$" means cranking around all the three axes. The upper and lower tables are for the triaxial deformation, $\gamma = 10^\circ$ and $20^\circ$, respectively.

| | no | $x$ | $y$ | $z$ | $xy$ | $yz$ | $zx$ | $xyz$ |
|---|---|---|---|---|---|---|---|---|
| $\gamma = 10^\circ$ | | | | | | | | |
| $E(2_1^+)$ (MeV) | 0.133 | 0.094 | 0.106 | 0.133 | 0.076 | 0.105 | 0.094 | 0.076 |
| $E(2_2^+)$ (MeV) | 1.742 | 1.732 | 1.735 | 1.237 | 1.722 | 1.226 | 1.221 | 1.216 |
| $B(E2)$ ($e^2$b$^2$) | 0.174 | 0.207 | 0.151 | 0.120 | 0.182 | 0.100 | 0.158 | 0.135 |
| $\gamma = 20^\circ$ | | | | | | | | |
| $E(2_1^+)$ (MeV) | 0.157 | 0.114 | 0.132 | 0.154 | 0.093 | 0.128 | 0.114 | 0.092 |
| $E(2_2^+)$ (MeV) | 0.498 | 0.481 | 0.494 | 0.349 | 0.474 | 0.347 | 0.330 | 0.324 |
| $B(E2)$ ($e^2$b$^2$) | 0.409 | 0.675 | 0.316 | 0.199 | 0.549 | 0.125 | 0.593 | 0.431 |

where the second $2^+$ excitation energy is reproduced. In contrast to the result shown in Fig. 2, the agreement with the experimental excitation energies at $\gamma = 12.8^\circ$ is much better; clearly indicating that the infinitesimal cranking improves the description of the $\gamma$ band. In Fig. 9 the calculated spectrum using the $xyz$-cranked HFB state with the triaxiality $\gamma = 12.8^\circ$ is compared with the experimental data, as in the case without cranking in Fig. 3. Apparently much better agreement with the experimental excitation energies for both the g band and the $\gamma$ band are obtained with this infinitesimal cranking procedure. It looks that the agreement of the $\gamma$ band becomes worse after $I \geqslant 14$. There is a reason for this: The band crossing occurs for the experimental $\gamma$ band. Namely, the $I \geqslant 14$ members are interpreted as the states generated by exciting the $\gamma$ vibration on the Stockholm band (s band), the lowest two-quasineutrons-aligned band, not on the g band. We do not include the s-band configuration in the present work and cannot describe the band crossing phenomenon in the $\gamma$ band.

To see the effect of the $xyz$ cranking on the transition probability, we show in Fig. 10 the calculated $B(E2)$ from the $0^+$ ground state to the second excited $2^+$ state in the $\gamma$ band as a function of the triaxiality $\gamma$. The prediction of the triaxial rotor model in Eq. (20) is also included with the calculated value of $B = 5.585$ ($e^2$b$^2$) in the case of the $xyz$ cranking. Compared to the result without cranking in Fig. 4, the general dependence of $B(E2)$ on $\gamma$ is similar; for example, the $B(E2)$ values seem to vanish at $\gamma \approx 27^\circ$ in both cases. Precisely speaking, however, the $B(E2)$ value does not vanish in the case with the $xyz$ cranking; this is because the amplitude $g^I_{K,\alpha}$ is complex in this case and the exact cancellation in Eq. (21) does not occur, although the imaginary part is very small so that the actual $B(E2)$ value almost vanishes. There are other marked differences: The position of the lower peak moves to higher $\gamma$ value, while that of the higher peak to lower $\gamma$ value, and the $B(E2)$ values at both peaks are slightly larger in the case with the $xyz$ cranking. The largest difference is observed at lower $\gamma$ values, $\gamma \lesssim 17^\circ$, where the $B(E2)$ value calculated with the $xyz$ cranking is smaller than that without cranking; e.g., it is less than half in $\gamma < 5^\circ$. The fact that the $B(E2)$ value with the $xyz$ cranking is larger than that without cranking in the range, $17.5^\circ \lesssim \gamma \lesssim 38^\circ$, and is smaller otherwise can be

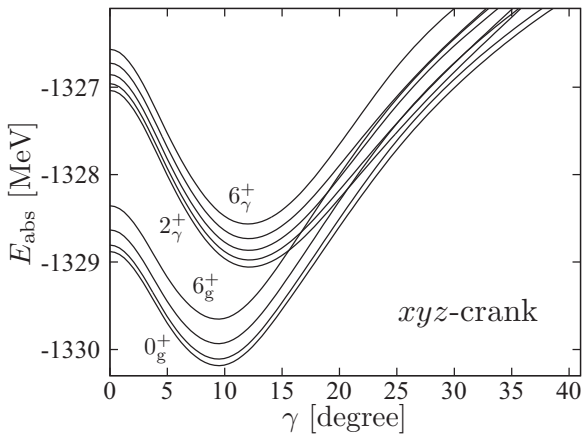


FIG. 7. Absolute energy curves as functions of the triaxial deformation parameter $\gamma$ calculated by the angular-momentum projection from the $xyz$-cranked HFB ground state in $^{164}$Er. Those for the $0^+$, $2^+$, $4^+$, and $6^+$ states of the g band and for the $2^+$, $3^+$, $4^+$, $5^+$, and $6^+$ states of the $\gamma$ band are included.

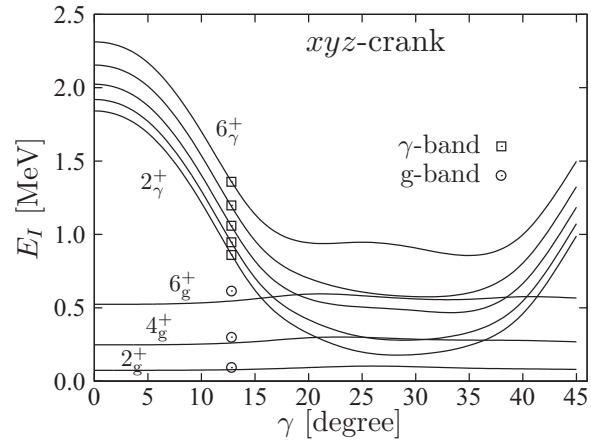


FIG. 8. Excitation energy curves as functions of the triaxial deformation parameter $\gamma$ calculated by the angular-momentum projection from the $xyz$-cranked HFB ground state in $^{164}$Er. Those for the $2^+$, $4^+$, and $6^+$ states of the g band and for the $2^+$, $3^+$, $4^+$, $5^+$, and $6^+$ states of the $\gamma$ band are included. Experimental data are also shown by symbols, open circles and squares, at $\gamma = 12.8^\circ$, where the calculated excitation energy of $2^+_\gamma$ coincides with the experimental one.

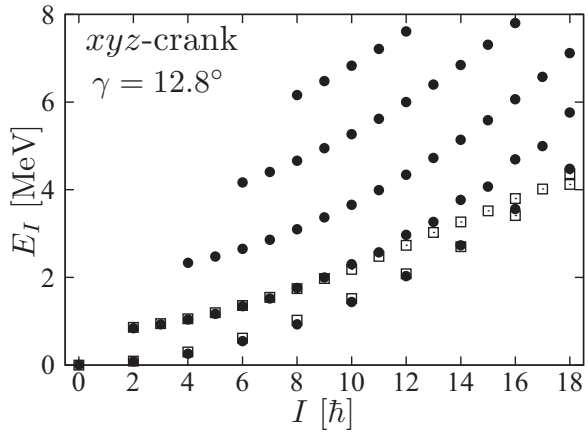


FIG. 9. Energy spectrum calculated by the angular-momentum projection from the $xyz$-cranked HFB state at $\gamma = 12.8^\circ$ in $^{164}$Er. The experimental data for the g band and the $\gamma$ band are included as open squares.

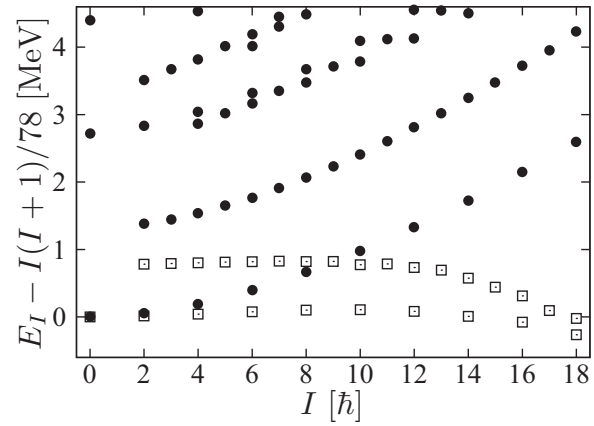


FIG. 11. Energy spectrum calculated by the angular-momentum-projected configuration-mixing using the five noncranked HFB states with $\gamma = 1^\circ$, $10^\circ$, $20^\circ$, $30^\circ$, and $40^\circ$ in $^{164}$Er. The rotational energy $I(I+1)/78$ MeV is subtracted. The experimental data for the g band and the $\gamma$ band are included as open squares.

seen also in Table I; the $B(E2)$ value reduces from 0.174 to 0.135 ($e^2$ b$^2$) at $\gamma = 10^\circ$, while it increases from 0.409 to 0.431 ($e^2$ b$^2$) at $\gamma = 20^\circ$. As discussed in the next section, the expected $\gamma$ value is not so large, $\gamma \lesssim 15^\circ$, and the effect of $xyz$ cranking appears to reduce the $B(E2)$ value, which makes the agreement better with the experimentally measured value.

### C. Configuration mixing for triaxial deformation

Until the previous section, the triaxiality $\gamma$ is a parameter and the results of the angular-momentum-projection calculation have been presented as a function of it; in some cases the appropriate value of $\gamma$ is searched to reproduce the experimental data. However, it should be determined theoretically, or it should be treated properly to make theoretical predictions

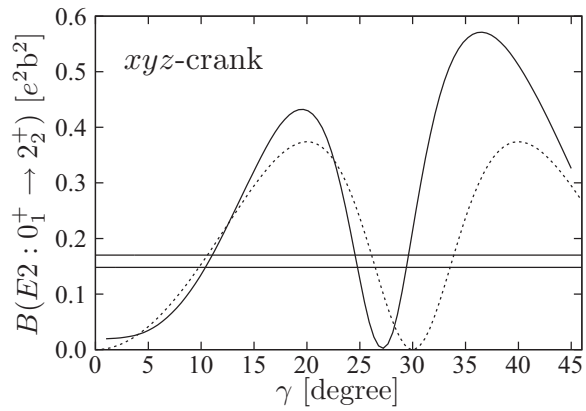


FIG. 10. $E2$ transition probability from the ground state to the second $2^+$ state as a function of the triaxial deformation parameter $\gamma$, which is calculated by the angular-momentum projection from the infinitesimally cranked HFB state around all the $xyz$ axes in $^{164}$Er (solid curve). The dotted curve is the prediction of the asymmetric rotor model [16] in Eq. (20), with $B = 5.585$ ($e^2$b$^2$). The experimentally measured values [27], 0.148 and 0.170 ($e^2$b$^2$), are shown by two horizontal lines.

independently of the experimental data. In this section we show the result of configuration-mixing with respect to the triaxiality parameter $\gamma$; namely, the final wave function is obtained by superposing the angular-momentum-projected states as in Eq. (7) in Sec. II A. Here five points have been employed for the $\gamma$ coordinate, $\gamma = 1^\circ, 10^\circ, 20^\circ, 30^\circ$, and $40^\circ$. We have checked that the excitation energies do not change within about 10 keV by increasing the number of HFB states from five in the range $0 < \gamma \lesssim 45^\circ$ at least for the low-lying states.

The resultant spectrum calculated by the configuration mixing superposing the five noncranked triaxial HFB states after the angular-momentum-projection is presented in Fig. 11, where the reference rotational energy is subtracted as in Figs. 5 and 6. In Fig. 12 the probability distributions [Eq. (9)] for the selected members of both the g band and the $\gamma$ band are shown. The distributions for the members of each band are quite similar, but those for the g band and for the $\gamma$ band are different; the average $\gamma$ value in the g band, $\approx 9^\circ$, is smaller than that in the $\gamma$ band, $\approx 15^\circ$; cf. Table II below.

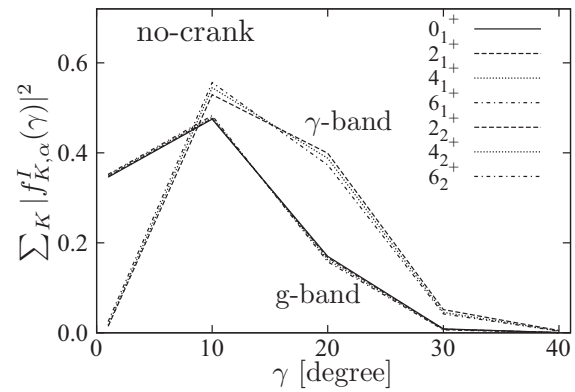


FIG. 12. The probability distributions of $0_1^+$, $2_1^+$, $4_1^+$, and $6_1^+$ states in the g band and $2_2^+$, $4_2^+$, and $6_2^+$ states in the $\gamma$ band with respect to the triaxiality parameter $\gamma$ for the configuration-mixing calculation of Fig. 11.

TABLE II. The excitation energies of the first and second $2^+$ states and the $B(E2: 0_1^+ \to 2_2^+)$ value calculated by the angular-momentum-projected configuration mixing with the infinitesimally cranked HFB states around various axes; e.g., "$yz$" means cranking around the $y$ and $z$ axes. The average triaxiality, $\langle\gamma\rangle$, and two times the standard deviation, $2\Delta\gamma = 2\sqrt{\langle(\gamma - \langle\gamma\rangle)^2\rangle}$, for the $0^+$ ground state and the $2^+$ $\gamma$ vibrational state are also included. The experimental data for the excitation energies and the $B(E2)$ value [27] are also tabulated at the last column.

| | no | $x$ | $y$ | $yz$ | $zx$ | $xyz$ | Exp. |
|---|---|---|---|---|---|---|---|
| $E(2_1^+)$ (MeV) | 0.137 | 0.090 | 0.100 | 0.099 | 0.089 | 0.078 | 0.091 |
| $E(2_2^+)$ (MeV) | 1.458 | 1.445 | 1.450 | 1.000 | 0.993 | 1.005 | 0.860 |
| $B(E2)$ ($e^2$b$^2$) | 0.222 | 0.259 | 0.202 | 0.137 | 0.200 | 0.180 | 0.148/0.170 |
| $\langle\gamma\rangle_{0_1^+}$ (°) | 8.8 | 8.8 | 8.8 | 8.8 | 8.8 | 8.8 | – |
| $2(\Delta\gamma)_{0_1^+}$ (°) | 13.8 | 13.8 | 13.8 | 13.8 | 13.8 | 13.8 | – |
| $\langle\gamma\rangle_{2_2^+}$ (°) | 15.1 | 15.1 | 15.0 | 13.7 | 13.7 | 13.8 | – |
| $2(\Delta\gamma)_{2_2^+}$ (°) | 12.8 | 12.8 | 12.8 | 12.1 | 12.1 | 12.1 | – |

These average $\gamma$ values are close to those which give minima of the absolute energies in Fig. 1; more precisely, $\gamma \approx 9.6°$ for the g band and $\gamma \approx 13.6°$ for the $\gamma$ band. Thus, the resultant triaxiality of the configuration-mixing is not so large, although the distribution with respect to $\gamma$ is considerably broad. From the spectrum shown in Fig. 11 one can see that the moments of inertia for both the g band and the $\gamma$ band are too small and deviation from the experimental data increases rapidly at higher spins. This is because the noncranked HFB states are employed. Moreover, the calculated excitation energy of the $\gamma$ vibration is too high, ≈1.46 MeV, compared with the experimental data, ≈0.86 MeV. Thus, the configuration mixing does not help to improve the moments of inertia or the excitation energy of the $\gamma$ vibration.

It should be mentioned that qualitative change of the calculated spectrum by the configuration-mixing is observed in Fig. 11 in comparison with, e.g., Fig. 5(a): New excited bands appear at higher excitation energy, for example, an even-$I$ band starting from the $0^+$ state at about 2.7 MeV. In this calculation with noncranked HFB states, this new band starting from the $0^+$ state almost degenerates with the band starting from the $4^+$ state at about 3.1 MeV (note that the reference rotational energy is subtracted in Fig. 11), both of which are interpreted as "two-phonon" $\gamma$ vibrational bands. In fact, the excitation energies of bandhead of these two bands are almost twice of that of the (one-phonon) $\gamma$ vibrational state. As it is well known, there are two two-phonon $\gamma$ vibrational states corresponding to the $K$ quantum numbers, $K = 0$ and $K = 4$. As discussed in Ref. [5], no $0^+$ excited band appears by the angular-momentum-projection from one triaxial mean-field state, which is exactly the feature of the asymmetric rotor model with the $(r_x, r_y, r_z) = (+1, +1, +1)$ $D_2$ symmetry [10]; this is also the case in our microscopic calculation. With the configuration mixing for the triaxial degree of freedom we additionally obtain the $0^+$ excited band. It may not be evident that this $0^+$ excited band can be interpreted as the $K = 0$ two-phonon $\gamma$ band. We have compared the three $E2$ transition probabilities, $B(E2: 0_1^+ \to 2_2^+)$, $B(E2: 2_2^+ \to 4_3^+)$ and $B(E2: 0_2^+ \to 2_2^+)$, which are $B(E2: 0_{\text{g.s.}}^+ \to 2_\gamma^+)$, $B(E2: 2_\gamma^+ \to 4_{\gamma\gamma}^+)$, and $B(E2: 0_{\gamma\gamma}^+ \to 2_\gamma^+)$, respectively, in an obvious notation, and all coincide in the harmonic vibrational limit [28]. The calculated values of these $B(E2)$'s are 0.222, 0.206, and 0.253 ($e^2$b$^2$), respectively; they are indeed close with each other. This result is in contrast to that of the other microscopic calculation in Ref. [15], where the calculated value of $B(E2: 0_{\gamma\gamma}^+ \to 2_\gamma^+)$ is considerably smaller than that of $B(E2: 2_\gamma^+ \to 4_{\gamma\gamma}^+)$. It is interesting to investigate how such a difference appears in the two microscopic calculations; it is, however, beyond the scope of the present work.

As for the moment of inertia and the excitation energy of the $\gamma$ vibrational band, the infinitesimal cranking plays an important role, as discussed in the previous section. We show the result of calculation by employing the five $xyz$-cranked triaxial HFB states with the same set of triaxiality parameters in Fig. 13 and the corresponding probability distribution in Fig. 14. Compared with the spectrum calculated without cranking in Fig. 11, a great improvement has been achieved by the infinitesimal cranking. The excitation energy of the $\gamma$ vibration, ≈1 MeV, becomes close to the experimental value. The moments of inertia for both the g band and the $\gamma$ band are considerably increased, although they are still slightly

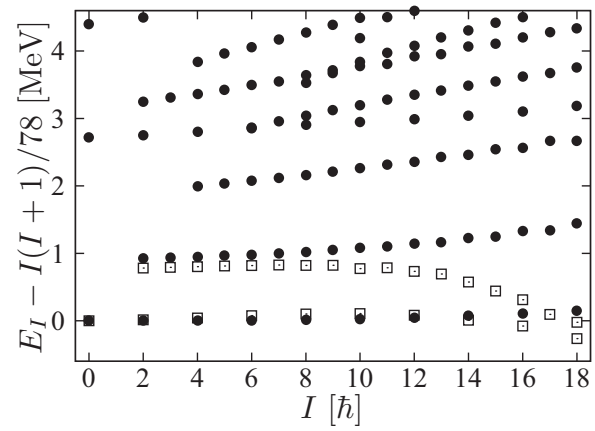


FIG. 13. Energy spectrum calculated by the angular-momentum-projected configuration-mixing using the five infinitesimally $xyz$-cranked HFB states with $\gamma = 1°, 10°, 20°, 30°$, and $40°$ in $^{164}$Er. The rotational energy $I(I+1)/78$ MeV is subtracted. The experimental data for the g band and the $\gamma$ band are included as open squares.

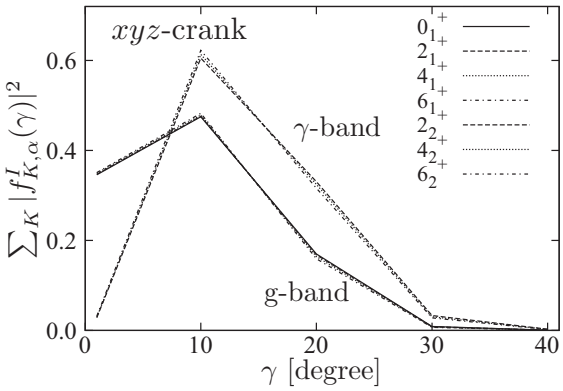


FIG. 14. The probability distributions of the $0_1^+$, $2_1^+$, $4_1^+$, and $6_1^+$ states in the g band and the $2_2^+$, $4_2^+$, and $6_2^+$ states in the $\gamma$ band with respect to the triaxiality parameter $\gamma$ for the configuration-mixing calculation of Fig. 13.

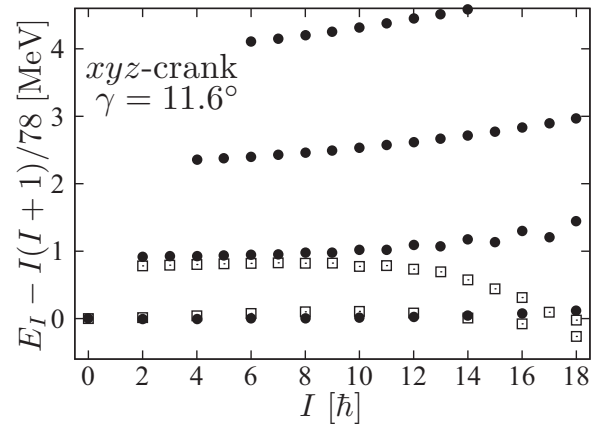


FIG. 15. Energy spectrum calculated by the angular-momentum projection from one $xyz$-cranked HFB state with $\gamma = 11.6^\circ$ in $^{164}$Er. The rotational energy $I(I+1)/78$ MeV is subtracted. The experimental data for the g band and the $\gamma$ band are included as open squares.

smaller at high-spin states. The experimentally observed moments of inertia increase as functions of spin, while the calculated inertias are rather constant in the present work. It was shown that the experimentally observed increasing feature of the moment of inertia can be well reproduced by superposing angular-momentum-projected configurations with different values of the cranking frequency [20]. It is, however, too heavy to perform the configuration-mixing calculations taking into account both the cranking frequency and the triaxial deformation at the same time. We believe further improvements can be obtained with such calculations. As for the probability distributions, those for the members of the g band are almost the same as in the case without cranking, while those for the members of the $\gamma$ band slightly move to lower $\gamma$ values and the widths of distribution become a little bit smaller by the effect of the $xyz$ cranking; cf. Table II.

Another interesting difference observed in Fig. 13 in comparison with Fig. 11 is that the degeneracy of the two bands interpreted as the two-phonon $\gamma$ bands with $K = 0$ and $K = 4$ is resolved by the $xyz$ cranking. The $0^+$ excited state at about 2.7 MeV keeps its excitation energy, while the third $4^+$ state becomes lower in energy from about 3.1 to 2.3 MeV (note that the reference rotational energy is subtracted in Figs. 11 and 13). With this effect the spectrum of the one- and two-phonon $\gamma$ vibrational states becomes similar to that in other calculations (see, e.g., Refs. [12,15]); namely, energies of the two-phonon states are larger than twice the energy of the one-phonon state, i.e., large anharmonicity is observed, and the $0^+$ state with $K = 0$ lies higher than the $4^+$ state with $K = 4$. The three $B(E2)$ values, $B(E2 : 0_1^+ \to 2_2^+)$, $B(E2 : 2_2^+ \to 4_3^+)$, and $B(E2 : 0_2^+ \to 2_2^+)$ are 0.180, 0.164, and 0.176 ($e^2$b$^2$), respectively, and so the interpretations of the $0^+$ and $4^+$ states as two-phonon $\gamma$ vibrational states may be justified also with the $xyz$ cranking.

To see the effect of superposing the five HFB states with different triaxial deformations, we show in Fig. 15 the calculated spectrum with a single HFB state with $\gamma = 11.6^\circ$, whose low-spin part of the $\gamma$ band roughly coincides with the result of configuration-mixing in Fig. 13. For the g band and the $\gamma$ band the resultant spectra in the two figures are very similar; as for these two bands the effect of the configuration mixing is not very large. However, other more excited bands are very different if Figs. 15 and 13 are compared. For example, excitation energies of the band starting from the $4_3^+$ state, interpreted as one of the excited two-phonon $\gamma$ bands, and of the band starting from the $6_4^+$, interpreted as a three-phonon band, are considerably lower in Fig. 13 than those in Figs. 15. Note that there are two almost completely degenerate $6^+$ states at about 3.4 MeV, which are at about 2.9 MeV in Fig. 13 because of the subtraction of the rotational energy, $I(I+1)/78$ MeV. Moreover, as already discussed, the band starting from the $0_2^+$ state, which is interpreted as another two-phonon band with strong anharmonicity, and the band from the $2_4^+$ state, which is interpreted as one of other three-phonon bands, etc., are missing in the angular-momentum-projection calculation from a single HFB state in Fig. 15. Therefore, the effect of configuration mixing is important for the complete understanding of the multiple

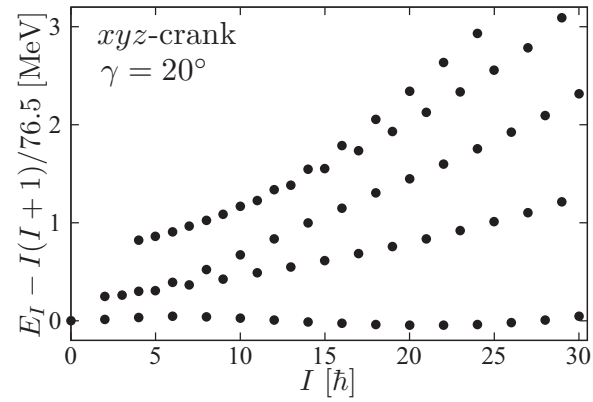


FIG. 16. Energy spectrum calculated by angular-momentum projection from the one $xyz$-cranked HFB state with the triaxial deformation, $\gamma = 20^\circ$, for $^{164}$Er, i.e., the same as Fig. 6(h) but its higher-spin part is shown. Only the five excited $|\Delta I| = 2$ bands from the lowest are shown.

$\gamma$ bands, although the experimental information of them, especially for the higher excited bands, is still scarce.

Although our best result is the one employing the infinitesimal cranking about all three axes, the $xyz$ cranking, we have performed the configuration-mixing calculations for some other cases. The results are summarized in Table II, where, for example, "$yz$" means that the five $yz$-cranked HFB states with the same set of triaxial deformations, $\gamma = 1^\circ$, $10^\circ$, $20^\circ$, $30^\circ$, and $40^\circ$, are superimposed. In this table, the average $\gamma$ values calculated by the probability distribution in Eq. (9),

$$\langle\gamma\rangle_\alpha \equiv \int \gamma\, p^I_\alpha(\gamma) d\gamma \approx \sum_n \gamma_n\, p^I_\alpha(\gamma_n), \tag{22}$$

and the two times the standard deviation, $2(\Delta\gamma)_\alpha \equiv 2\sqrt{\langle(\gamma - \langle\gamma\rangle_\alpha)^2\rangle_\alpha}$, which roughly corresponds to the full width at half maximum, are also included. The basic feature is the same as that in the result of calculation with using a single HFB state: The moment of inertia reflected by the first $2^+$ energy is increased mainly by the $x$- and $y$-axis cranking, and the second $2^+$ (i.e., the $\gamma$ vibrational) energy is lowered mainly by the $z$-axis cranking. The $B(E2)$ value is increased by the $x$ cranking, while it is decreased by the $y$- and $z$-axis cranking. These features are specific for the case where the triaxial deformation is relatively small. In fact, the average $\gamma$ values are about $9^\circ$ for the g band and about $13^\circ$–$15^\circ$ for the $\gamma$ band. It may be worthwhile noticing that the infinitesimal cranking about more than two axes makes the average $\gamma$ value and the width of distribution smaller for the $\gamma$ band, while those for the g band are not affected.

As for the rotational in-band $E2$ transitions for the g band, the result is similar to that of our previous axially symmetric calculation in Ref. [20] and agrees very well with the experimental data. The reason is that the deformation parameter $\beta_2$ is very similar and the triaxiality is rather small in the g band. Precisely speaking, the $B(E2)$ value is about 2% larger than that in Ref. [20] at low spins and the difference gradually increases up to about 10% at $I \approx 20$, where there are no experimental data available. Thus, the effect of configuration mixing for the triaxial deformation does not have a large impact for the $E2$ transitions inside the g band.

### D. Relation to wobbling motion

It was suggested in Ref. [29] that a character change from the $\gamma$ vibration to the wobbling motion is expected in the high-spin continuation of the $\gamma$ band. In fact, in the result of calculation with the larger triaxial deformation, $\gamma = 20^\circ$, the signature-splitting of the multiphonon excited bands becomes large at high spins and the even-$I$ and odd-$I$ sequences alternately compose a different type of multiple band structure from the one at low spins, as clearly seen in Figs. 6(c), 6(d), and 6(f). We take the example of this calculation with $\gamma = 20^\circ$ and briefly discuss the character change in the following, although it does *not* correspond to the experimental situation of $^{164}$Er: More complete discussion will be reported in a separate publication.

We show the higher-spin continuation of the result of the $xyz$ cranking in Fig. 6(h), where a slightly different rotational energy from that in Fig. 6 is subtracted to make the yrast band as flat as possible. It can be seen that a nice wobblinglike multiple band structure develops at $I \gtrsim 20$; the yrast band is composed of the even-$I$ states, the first excited band is of the odd-$I$, the second excited band is of the even-$I$, and so on. The excitation energy of the first excited band increases almost linearly as a function of spin as it is expected [10]. It may be interesting to notice that the spectrum is not exactly phononlike in the sense that the excitation energy from the $(n-1)$th excited band to the $n$th band decreases as $n$ increases ($n = 1,2,3,\ldots$).

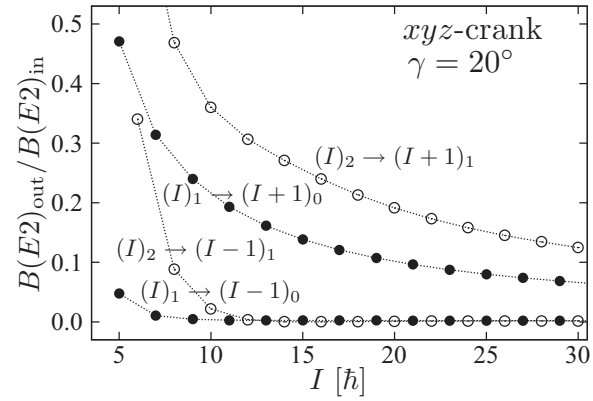


FIG. 17. The $B(E2)$ ratio of the out-of-band to the in-band transitions, $B(E2: I \to I \pm 1)/B(E2: I \to I-2)$, for the first and the second excited bands in the wobblinglike structure in Fig. 16. The solid (open) symbols denote the transitions from the first (second) band.

The ratios of $E2$ transition probabilities, the out-of-band to the in-band, $B(E2: I \to I \pm 1)/B(E2: I \to I-2)$, are shown as functions of spin in Fig. 17 for the first and second excited bands. The large out-of-band transition is one of the characteristic features of the wobbling band, which is, in fact, employed as a guide to identify it in experiments. As is seen in the figure, the out-of-band transitions are indeed very large, as expected. It should be mentioned that there are two types of out-of-band transitions: One is the $I \to I+1$ transition and another is the $I \to I-1$ transition (cf. Ref. [30]), and the former transitions are one or two orders of magnitude larger in the present case. One might wonder why; the reason is that the main rotation axis is the $y$ axis in the present case. The three nuclear moments of inertia behave like those of the irrotational flow liquid, and the largest inertia is that of the middle axis, which is the $y$ axis, as mentioned in Eq. (18). Namely, the rotation of the present example is of the so-called "negative-$\gamma$" scheme, where nucleus rotates mainly about the middle axis, in contrast to the "positive-$\gamma$" scheme with the main rotation about the shortest axis. Note that if the axis of rotation is chosen to be the $x$ axis, as is usually done in the study of high-spin states [31], the positive-$\gamma$ and negative-$\gamma$ rotation schemes correspond to the triaxial shape with $0 < \gamma < 60^\circ$ and $-60^\circ < \gamma < 0$, respectively, from which the naming of them comes.

To confirm that the main rotation axis is the $y$ axis in the present example, the expectation value of the angular momentum vector should be calculated in the body-fixed frame, which is nontrivial at all for angular-momentum-projected

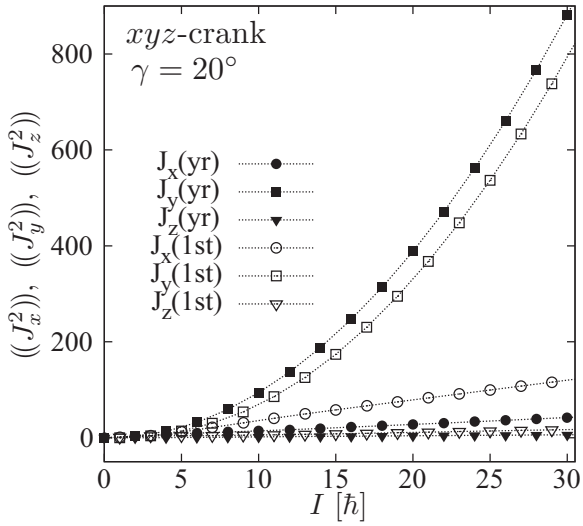


FIG. 18. The "expectation values" of the squared $x,y,z$ components of the angular momentum vector in the body-fixed frame, which are defined by Eq. (23), for the yrast band (solid symbols) and for the first excited band (open symbols) in Fig. 16.

wave functions. In Ref. [32] the result of such a calculation have been shown, but, unfortunately, how to calculate is not explained. In the present work, following the rotor model and using the microscopically calculated normalized amplitudes $\{f^I_{K,\alpha}\}$ in Eq. (6), we define the expectation value of the squared intrinsic component $J_i^2$ for the projected eigenstate $\alpha$ as

$$\left(\left(J_i^2\right)\right)_\alpha \equiv \sum_{K\,K'} f^{I*}_{K,\alpha}\,\langle I\,K|J_i^2|I\,K'\rangle\,f^I_{K',\alpha}, \tag{23}$$

where $i = x,y,z$ denotes the axis of the body-fixed frame specified by the deformed mean-field wave function $|\Phi\rangle$, from which the projection is performed. Needless to say, the purely algebraic quantity $\langle I\,K|J_i^2|I\,K'\rangle$ should be manipulated in the intrinsic frame. The expectation values thus calculated for the yrast band and for the first excited band are shown in Fig. 18 as functions of spin. Apparently, the main rotation axis is the $y$ axis; those of the $x$ and $z$ components increase almost linearly as functions of spin, which is a typical behavior for the angular momentum fluctuations.

## IV. SUMMARY AND DISCUSSION

In the present work, we have investigated the infinitesimal cranking of the mean-field wave function to improve the description of the collective rotational motion by means of the angular-momentum-projected method. For the triaxial deformation there are three axes for cranking. Assuming the totally $D_2$ symmetric mean-field wave function before the cranking, it is clarified what kind of different time-odd components are induced into the wave function by the cranking about these three axes; they are classified according to the $D_2$ symmetry quantum numbers $(r_x,r_y,r_z)$.

Taking a nucleus $^{164}$Er as a typical example in the rare-earth region, we have first studied the spectrum and the $B(E2)$ values by the angular-momentum-projection from a single HFB state without cranking assuming the triaxial deformation. The Gogny D1S force is employed as an effective interaction and there is no adjustable parameter in the Hamiltonian. As in the pioneering work of Ref. [5], the multiple $\gamma$ bands appear in addition to the g band by including the triaxial deformation into the mean-field wave function. The $\gamma$ dependencies of the microscopically calculated energy spectrum and $B(E2)$ values are similar to those of the asymmetric rotor model with the irrotational moments of inertia at least for $5^\circ \lesssim \gamma \lesssim 30^\circ$. It has been found, however, that the moments of inertia for both the g band and the $\gamma$ band are too small compared with the experimental data, and, moreover, rather large triaxial deformation is necessary to reproduce the low-lying nature of the $\gamma$ vibration, with which the $B(E2)$ value from the g band to the $\gamma$ band is largely overestimated. These problems of the result of the projection from a single HFB state without cranking are shown to be greatly improved if the infinitesimal cranking around all three axes is performed for the mean-field wave function. The effects of the infinitesimal cranking around the three axes are quite different: For $\gamma = 10^\circ$ and $\gamma = 20^\circ$ the $x$- and $y$-axis cranking mainly increase the moments of inertia and the $z$-axis cranking decreases the excitation energy of the $\gamma$ vibration; furthermore, it was found that the $y$-axis cranking increases the signature splitting between the even-$I$ and the odd-$I$ sequences of the $\gamma$ band, while the $x$-axis cranking decreases it. With the infinitesimal cranking about all three axes a reasonable agreement for both the spectrum and $B(E2)$ can be achieved with relatively small triaxial deformation $\gamma \approx 12^\circ$.

To see what is the most probable triaxial deformation, we next performed the angular-momentum-projected configuration-mixing calculation by superposing several HFB states with different triaxial deformations. The average $\gamma$ values for the g band and the $\gamma$ band are slightly different; they are about $9^\circ$ and $14^\circ$, respectively, which are not so large and are comparable to the amplitude of the zero-point oscillation estimated by the measured $B(E2)$ value [10]: In fact, the calculated width of the distributions for the triaxial deformation is about $12^\circ$–$14^\circ$. Thus, it does not conflict with the usual belief that the ground-state deformation is axially symmetric in the rare-earth region. With these calculated distributions for the triaxial deformation, the resultant spectrum and the $B(E2)$ value agree reasonably well with the experimental data, although the agreement is not perfect. This is in contrast to the result of the RPA calculation [12]: If the excitation energy is reproduced, the $B(E2)$ value is largely overestimated by a factor 2–4. Our calculation gives a correct magnitude if the amplitude for the triaxial deformation is properly determined by the configuration mixing. It should be stressed that several new bands appear at higher excitation energy by the configuration mixing. Especially the $K = 0$ two-phonon band, which is missing in the projection calculation from a single HFB state, emerges above the $K = 4$ two-phonon band; this anharmonic pattern is very similar to what was predicted by other calculations; cf., e.g., Refs. [12–15].

Finally, we have investigated the conjecture of Ref. [29] that the multiple $\gamma$ bands change their character into the wobbling band. By the hypothetical calculation with relatively large triaxial deformation, $\gamma = 20^\circ$, for $^{164}$Er, it has been found that indeed the character change occurs and the high-spin part of

the multiple $\gamma$ bands can be interpreted as the wobbling band. The characteristic features of the calculated wobbling motion are studied: The excitation energy of the wobbling phonon almost linearly increases as a function of spin and the strong $I \to I+1$ out-of-band $E2$ transitions are predicted, which are expected in the original work of the wobbling motion [10] for the so-called negative-$\gamma$ rotation scheme [30]. In experiment the wobbling band had been first observed in the odd nucleus, $^{163}$Lu, in the rare-earth region. Interestingly enough, however, the experimentally observed properties are opposite from what are predicted in the present calculation. The excitation energy decreases as spin increases, which is now understood as the characteristic feature of the so-called "transverse" wobbling [33], and only the $I \to I-1$ out-of-band $E2$ transitions are measured, which is characteristic for the so-called positive-$\gamma$ rotation scheme [30]. It should be pointed out that the possible occurrence of the transverse wobbling was first pointed out in Ref. [34], where the effect of the aligned angular momentum of the odd particle on the wobbling excitation energy was carefully examined. We have also studied the wobbling motion in $^{163}$Lu by the angular-momentum-projection method, and the preliminary result was reported in Ref. [35], where the expected properties for the case of $^{163}$Lu are reproduced, although the agreement with the experimental data is not very satisfactory. Thus, the wobbling motion that appeared in the present hypothetical calculation is somewhat different from what is observed in experiment. We would like to notice, however, that the observed excitation energy of the two-phonon wobbling state in $^{163}$Lu is smaller than twice the energy of the one-phonon state [36], which roughly corresponds to what is seen in the result of present calculation. We have been investigating the wobbling motion in $^{163}$Lu by performing similar calculation to the present work; the result will be reported in a separate publication.

## ACKNOWLEDGMENTS

Discussion with Professor Yang Sun, when he visited Kyushu University, is greatly appreciated. This work is supported in part by Grant-in-Aid for Scientific Research (C) No. 25.949 from Japan Society for the Promotion of Science.

## APPENDIX: EXPECTATION VALUE IN THE INTRINSIC FRAME

There is no concept of the intrinsic frame or the body-fixed frame for the angular-momentum-projected wave function in Eq. (1). Therefore, the expectation value of some operator in the intrinsic frame is not an observable quantity and should be *defined* in some way. In the text we have used the definition by Eq. (23) for the squared component of the angular momentum vector, but this definition solely relies on the macroscopic rotor model and can be applied only for the angular momentum operator without any additional assumptions. It is desirable to calculate the expectation value of an arbitrary operator microscopically. In this Appendix we present some attempt following again the basic idea of the rotor model; the components of the spherical tensor operator in the body-fixed frame are scalar and commute with the rotation operator. For an arbitrary scalar observable $\mathcal{O}$ the expectation value with respect to the projected wave function in Eq. (1) is written, just like for the Hamiltonian, as

$$\langle \Psi^I_{M,\alpha} | \mathcal{O} | \Psi^I_{M,\alpha} \rangle = \sum_{KnK'n'} g^{I*}_{Kn,\alpha} \langle \Phi_n | \mathcal{O} P^I_{KK'} | \Phi_{n'} \rangle \, g^I_{K'n',\alpha}. \tag{A1}$$

Of course, it does not depend on the $M$ quantum number. However, if the observable $\mathcal{O}$ does not commute with the projector, the right-hand side is generally complex, so that one has to take the real part or symmetrize; thus, we define the expectation value by

$$\begin{aligned} \langle\!\langle \mathcal{O} \rangle\!\rangle_\alpha &\equiv \mathrm{Re}\left( \sum_{KnK'n'} g^{I*}_{Kn,\alpha} \langle \Phi_n | \mathcal{O} P^I_{KK'} | \Phi_{n'} \rangle \, g^I_{K'n',\alpha} \right) \\ &= \frac{1}{2} \sum_{KnK'n'} g^{I*}_{Kn,\alpha} \langle \Phi_n | (\mathcal{O} P^I_{KK'} + P^I_{KK'} \mathcal{O}) | \Phi_{n'} \rangle \\ &\quad \times g^I_{K'n',\alpha}, \end{aligned} \tag{A2}$$

where because of this specific definition, we have used the notation, $\langle\!\langle \mathcal{O} \rangle\!\rangle_\alpha$, instead of a usual single bracket, and the amplitudes $\{g^I_{Kn,\alpha}\}$ are assumed to be normalized.

Then the expectation value of the squared intrinsic component $J_i^2$ can be microscopically calculated by

$$\left\langle\!\!\left\langle J_i^2 \right\rangle\!\!\right\rangle_\alpha \equiv \mathrm{Re}\left( \sum_{KK'} g^{I*}_{K,\alpha} \langle \Phi | J_i^2 \, P^I_{KK'} | \Phi \rangle \, g^I_{K',\alpha} \right), \tag{A3}$$

where the configuration-mixing is neglected for simplicity and the projection is performed from a single HFB state $|\Phi\rangle$. This expression is a microscopic analog of Eq. (23), in which the concept of the rotor model is fully employed. In Fig. 19 we compare the results of two definitions, Eqs. (23) and (A3),

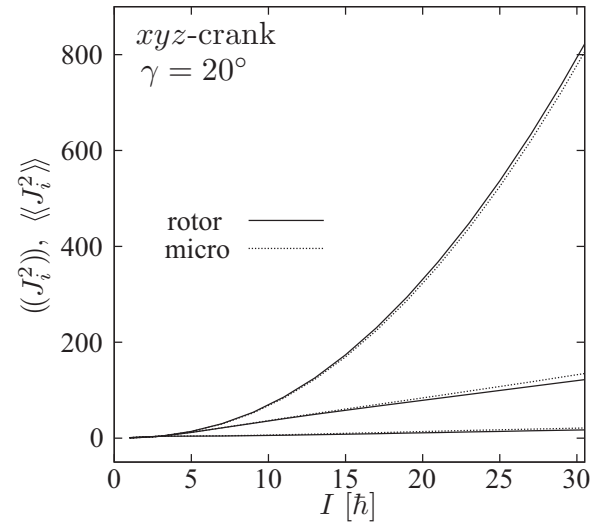


FIG. 19. Comparison of the two definitions for the "expectation values" of the squared components of the angular momentum vector in the body-fixed frame for the first excited band in Fig. 16, which are calculated by Eq. (23) (solid lines) and by Eq. (A3) (dotted lines). The solid lines are the same as those with the open symbols in Fig. 18.

for the first excited band considered in Sec. III D (the result for the ground-state band is similar). The agreement of these two definitions is clear from the figure, and the definition in Eq. (A3) seems to be meaningful: However, it is not always the case. In fact, the operators $J_i^2$ $(i = x,y,z)$ are not scalar but a part of the second rank tensor, $X_{ij} \equiv \frac{1}{2}(J_i J_j + J_j J_i)$. We have found that the expectation value of the nondiagonal part, e.g., $\langle\langle X_{yz}\rangle\rangle_\alpha$, depends on the infinitesimal frequencies $(\omega_x,\omega_y,\omega_z)$, and therefore can take arbitrary values [$\langle\langle X_{ij}\rangle\rangle_\alpha = 0$ $(i \neq j)$ without cranking]. It can be confirmed that the diagonal part, $\langle\langle J_i^2\rangle\rangle_\alpha$, is independent of these frequencies by using the $D_2$ symmetry; the mean-field wave function before the cranking is totally $D_2$ symmetric in the present case. Therefore, the definition in Eq. (A2) does not always work.


[1] P. Ring and P. Schuck, *The Nuclear Many-Body Problem* (Springer, New York, 1980).
[2] S. Tagami and Y. R. Shimizu, Prog. Theor. Phys. **127**, 79 (2012).
[3] S. Tagami, Y. R. Shimizu, and J. Dudek, Phys. Rev. C **87**, 054306 (2013).
[4] S. Tagami, Y. R. Shimizu, and J. Dudek, J. Phys. G **42**, 015106 (2015).
[5] Y. Sun, K. Hara, J. A. Sheikh, J. G. Hirsch, V. Velázquez, and M. Guidry, Phys. Rev. C **61**, 064323 (2000).
[6] J. A. Sheikh, G. H. Bhat, Y. Sun, G. B. Vakil, and R. Palit, Phys. Rev. C **77**, 034313 (2008).
[7] K. Hara and Y. Sun, Int. J. Mod. Phys. E **04**, 637 (1995).
[8] V. Velázquez, J. Hirsch, and Y. Sun, Nucl. Phys. A **643**, 39 (1998).
[9] J. M. Eisenberg and W. Greiner, *Nuclear Models* (North Holland, Amsterdam, 1970), Vol. I.
[10] A. Bohr and B. R. Mottelson, *Nuclear Structure* (Benjamin, New York, 1975), Vol. II.
[11] D. R. Bés, P. Federman, E. Mqaueda, and A. Zuker, Nucl. Phys. **65**, 1 (1965).
[12] T. S. Dumitrescu and I. Hamamoto, Nucl. Phys. A **383**, 205 (1982).
[13] M. Matsuo and K. Matsuyanagi, Prog. Theor. Phys. **74**, 1227 (1985).
[14] M. Matsuo and K. Matsuyanagi, Prog. Theor. Phys. **76**, 93 (1986).
[15] M. Matsuo and K. Matsuyanagi, Prog. Theor. Phys. **78**, 591 (1987).
[16] A. S. Davydov and F. G. Filippov, Nucl. Phys. A **8**, 237 (1958).
[17] T. Shoji, Ph.D. thesis, Department of Physics, Kyushu University, April 2009.
[18] J. F. Berger, M. Girod, and D. Gogny, Comput. Phys. Commun. **63**, 365 (1991).
[19] A. Staszczak, M. Stoitsov, A. Baran, and W. Nazarewicz, Eur. Phys. J. A **46**, 85 (2010).
[20] M. Shimada, S. Tagami, and Y. R. Shimizu, Prog. Theor. Exp. Phys. **2015**, 063D02 (2015).
[21] A. Kerman and N. Onishi, Nucl. Phys. A **361**, 179 (1981).
[22] S. Frauendorf, Rev. Mod. Phys. **73**, 463 (2001).
[23] A. Hayashi, K. Hara, and P. Ring, Phys. Rev. Lett. **53**, 337 (1984).
[24] K.-I. Enami, K. Tanabe, N. Yoshinaga, and K. Higashiyama, Prog. Theor. Phys. **104**, 757 (2000).
[25] Y. R. Shimizu, T. Shoji, and M. Matsuzaki, Phys. Rev. C **77**, 024319 (2008).
[26] Y. R. Shimizu and K. Matsuyanagi, Prog. Theor. Phys. **71**, 960 (1984).
[27] R. M. Ronningen, R. S. Grantham, J. H. Hamilton, R. B. Piercey, A. V. Ramayya, B. van Nooijen, H. Kawakami, W. Lourens, R. S. Lee, W. K. Dagenhart, and L. L. Riedinger, Phys. Rev. C **26**, 97 (1982).
[28] A. Bohr and B. R. Mottelson, Phys. Scr. **25**, 28 (1982).
[29] I. N. Mikhailov and D. Janssen, Phys. Lett. B **72**, 303 (1978).
[30] Y. R. Shimizu and M. Matsuzaki, Nucl. Phys. A **588**, 559 (1995).
[31] G. Andersson, S. E. Larsson, G. Leander, P. Möller, S. G. Nilsson, I. Ragnarsson, S. Åberg, J. Dudek, B. Nerlo-Pomorska, K. Pomorski, and Z. Szymański, Nucl. Phys. A **268**, 205 (1976).
[32] Zao-Chun Gao, Y. S. Chen, and Yang Sun, Phys. Lett. B **634**, 195 (2006).
[33] S. Frauendorf and F. Dönau, Phys. Rev. C **89**, 014322 (2014).
[34] Y. R. Shimizu, M. Matsuzaki, and K. Matsuyanagi, Microscopic study of wobbling motions in Hf and Lu nuclei, in *Proceedings of the Fifth Japan-China Joint Nuclear Physics Symposium*, April 2004, pp. 317–326, arXiv:nucl-th/0404063v1.
[35] S. Tagami, M. Shimada, Y. Fujioka, Y. R. Shimizu, and J. Dudek, in Proceeding of the 2013 Kazimierz International Conference, September 2013; Phys. Scr. **89**, 054013 (2014).
[36] D. R. Jensen *et al.*, Phys. Rev. Lett. **89**, 142503 (2002).